Research article

JHEP|Reports

Salsalate improves the anti-tumor efficacy of lenvatinib in MASH-driven hepatocellular carcinoma

Authors

Evangelia E. Tsakiridis, Elham Ahmadi, Jaya Gautam, …, Paola Muti, Theodoros Tsakiridis, Gregory R. Steinberg

Correspondence

gsteinberg@mcmaster.ca (G.R. Steinberg).

Graphical abstract

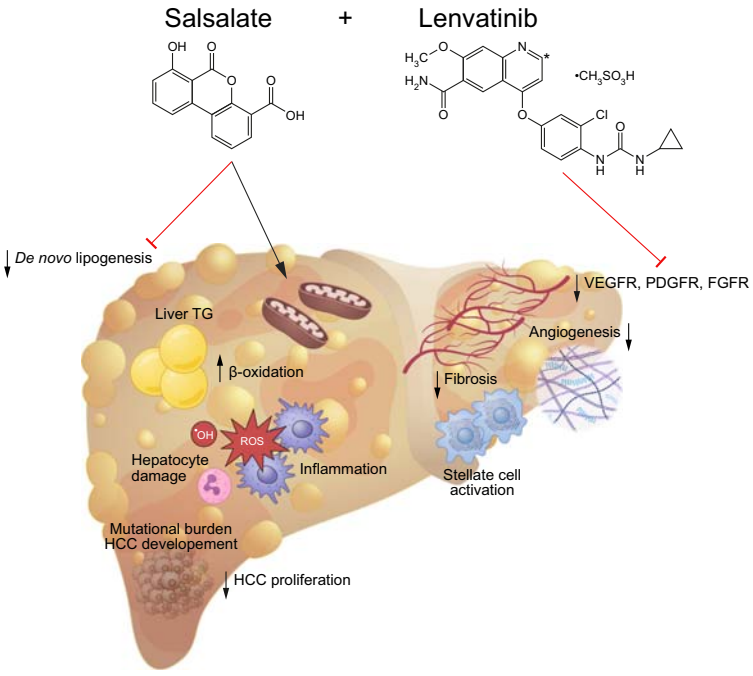

Highlights:

- Clinically relevant concentrations of LEN and SAL synergistically suppressed the proliferation and clonogenic survival of HCC cells.
- These effects were associated with activation of AMPK and inhibition of the mTOR-HIF1a and Erk1/2 signaling pathways.
- SAL combined with LEN enhanced survival in an orthotopic xenograft model of HCC.
- Regulatory network analysis results suggest a potential role for ATF3 and ETS1.
- These results have significant translational potential, given the favorable safety profile of SAL.

Impact and implications:

Although rates of MASH-HCC are on the rise globally, standard-of-care multi-tyrosine kinase inhibitors and immunotherapy have limited efficacy in this HCC etiology. Metabolic targeting with SAL inhibits cancer growth kinetics while also alleviating drivers of MASH by increasing fatty acid oxidation and reducing *de novo* lipogenesis and fibrosis. Combined LEN and SAL improved survival and MASH-HCC pathology in mouse models without adverse effects. Given that SAL is a safe, economical, and approved medication, this concept holds great translational potential that could provide a new treatment avenue for patients with unresected MASH-HCC.

https://doi.org/10.1016/j.jhepr.2025.101354

 JHEP Reports, 2025, 7, 1–17

Research article

JHEP|Reports

Salsalate improves the anti-tumor efficacy of lenvatinib in MASH-driven hepatocellular carcinoma

Evangelia E. Tsakiridis[1,2], Elham Ahmadi[1,3], Jaya Gautam[1,2], Yi Ran Hannah She[1,2], Russta Fayyazi[1,2], James S.V. Lally[1,2], Simon Wang[1,3,4], Fiorella Di Pastena[1,2], Celina M. Valvano[1,2], Daniel Del Rosso[1,2,4], Olga-Demetra Biziotis[1,3,4], Brandon Meyers[3,4], Paola Muti[1,2,4], Theodoros Tsakiridis[1,3,4], Gregory R. Steinberg[1,2,*]

JHEP Reports **2025**. vol. 7 | 1–17

Background & Aims: Metabolic dysfunction-associated steatohepatitis (MASH) is a growing cause of hepatocellular carcinoma (HCC) worldwide. The complex microenvironment of these tumors, characterized by metabolic dysfunction, hypoxia, steatosis, and fibrosis, limits the effectiveness of standard-of-care therapies, such as the multi-tyrosine kinase inhibitor lenvatinib (LEN). Salsalate (SAL), is a rheumatoid arthritis therapy that enhances fatty acid oxidation and reduces *de novo* lipogenesis, fibrosis and cell proliferation pathways. We hypothesize that addition of SAL could improve the efficacy of LEN in MASH-HCC.

Methods: We assessed the efficacy of combination therapy using clinically relevant concentrations of LEN and SAL in human HCC cell models, orthotopic xenograft and MASH-HCC mouse models. In addition, assays assessing fatty acid oxidation and lipogenesis, protein immunoblotting and RNA-sequencing were used to understand mechanisms involved.

Results: LEN + SAL synergistically suppressed the proliferation and clonogenic survival of cells ($p \leq 0.0001$), prolonged survival in an orthotopic xenograft model ($p = 0.02$), and reduced angiogenesis, fibrosis, and steatosis ($p \leq 0.05$) in a MASH-HCC model. These effects were associated with activation of AMPK and inhibition of the mTOR-HIF1α and Erk1/2 signaling pathways. RNA-sequencing analysis in both Hep3B cells and livers of the MASH-HCC mouse model revealed that SAL enhanced fatty acid oxidation and suppressed fibrosis and cell cycle progression, while LEN reduced angiogenesis with regulatory network analysis, suggesting a potential role for activating transcription factor 3 (ATF3) and ETS-proto-oncogene-1 (ETS-1).

Conclusions: These data indicate that combining LEN and SAL, which exert distinct effects leading to improvements in the liver microenvironment (steatosis, angiogenesis, and fibrosis) and inhibition of tumor proliferation, may have therapeutic potential for MASH-driven HCC.

Introduction

The incidence of hepatocellular carcinoma (HCC) is increasing, in part, due to the epidemic of metabolic-associated steatohepatitis (MASH).[1–3] Based on prevalence of obesity and type 2 diabetes mellitus, mathematical modeling predicts a striking 130% increase in cases of MASH-related HCC between 2016 and 2030.[4] Despite its high prevalence, MASH-driven HCC is often diagnosed at an advanced and inoperable stage, and has limited therapeutic options and a low 5-year survival rate of 19%.[5] Accumulation of driver mutations, such as *TERT*, *CTNNB1*, and *TP53*, and the complex MASH–liver microenvironment, characterized by inflammation and fibrosis, promote drug and immunotherapy resistance.[6]

Current first-line therapies for advanced unresectable HCC include multi-tyrosine kinase inhibitors, such as lenvatinib (LEN), and immunotherapies, for example the atezolizumab–bevacizumab combination targeting PD-L1 and VEGF, respectively.[7,8] However, meta-analysis of the CheckMate-459, KEYNOTE-240, and IMbrave-150 trials demonstrated that immunotherapy did not offer a survival advantage in the subgroup of patients with non-viral HCC.[9] Similarly, immunotherapy did not provide superior prognostic outcomes in non-viral HCC in the COSMIC-312 Phase III trial,[10] or following a retrospective multicenter analysis in patients with non-viral advanced HCC treated with atezolizumab–bevacizumab, LEN, or sorafenib.[11,12] The above findings highlight the importance of LEN as a treatment in MASH-associated HCC and the need to develop new strategies to maximize its therapeutic ratio. One such strategy is to target key pathological features of MASH-HCC progression, including steatosis, angiogenesis, and inflammation, which lead to metabolic dysfunction and fibrosis.

Salsalate (SAL), a dimer of salicylate, is an anti-inflammatory drug used for treatment of rheumatoid arthritis. It is well tolerated at an oral dose of 3–5 g/day, which yields maximal plasma concentrations of salicylate of 1–3 mM.[13] Upon absorption, it is cleaved into salicylate, which, unlike acetylsalicylate (aspirin), is not associated with gastrointestinal bleeding risk.[14] In patients

* Corresponding author. Address: Centre for Metabolism, Obesity and Diabetes Research, McMaster University, 1280 Main Street West, Hamilton, ONT, L8S 4K1, Canada.
E-mail address: gsteinberg@mcmaster.ca (G.R. Steinberg).
https://doi.org/10.1016/j.jhepr.2025.101354

with insulin resistance and/or type 2 diabetes mellitus, SAL has been demonstrated to lower fasting glucose,[15–19] triglyceride levels,[17,18,20] and markers of inflammation.[15,17–20] In preclinical animal models of MASH, clinically achievable doses of SAL were shown to improve glucose homeostasis and reduce liver steatosis.[21] These effects of SAL are mediated through activation of the AMP-activated protein kinase (AMPK)[21,22] and mitochondrial uncoupling, both of which increase fatty acid oxidation (FAO) and reduce liver *de novo* lipogenesis (DNL).[21] AMPK is also a favorable target in MASH because of its ability to suppress inflammation and fibrosis while stimulating autophagy and mitochondrial homeostasis, as well as its effects on FAO and DNL.[23–25] In addition to metabolic reprogramming in the liver, SAL also exerts anti-tumor properties in mouse models of lung and prostate cancer.[26–28]

Given the positive effects of SAL on the carcinogenesis-prone liver microenvironment and its antiproliferative effects on tumors, we hypothesized that SAL would enhance the therapeutic ratio of LEN in MASH-driven HCC. Thus, we investigated the effects of clinically achievable doses of a combination of LEN + SAL (COMBO) on animal survival and markers of liver steatosis, fibrosis, and angiogenesis in mouse models of HCC.

Materials and methods

Cell culture

Immortalized HCC lines

Hep3B, PLC PRF/5, and HEPG2 cells were obtained from American Type Culture Collection (ATCC) and maintained in Eagles Minimum Essential Media (EMEM) (Wisent, Saint-Jean-Baptiste, Canada, Cat # 320-026-CL) or Dulbecco's Modified Eagle Medium (DMEM) (Wisent, Cat #319005) for HUH7 cells. All lines were supplemented with 1% antibiotic–antimycotic (Wisent, Cat # 450-115-ELP) and 10% FBS (Wisent, Cat # 098150) at 37 °C and 5% CO_2. Cells were passaged using 0.25% trypsin-EDTA solution (Wisent, Cat # 325-043-CL). Hep-3B-Luc-1 were generated by transfecting cells with a luciferase reporter.

Immortalized MEF lines

AMPK $\beta1^{+/+}$ (WT) or AMPK $\beta1^{-/-}$ murine embryonic fibroblasts (MEFs) isolated from mouse embryos at embryonic day (E) 13.5 were generated as previously described[29] and immortalized by continuous passaging. Cells were cultured in DMEM (25 mM glucose) containing 10% FBS, 4 mM L-glutamine, 1 mM sodium pyruvate, 1x antibiotic/antimycotic solution, and 1x nonessential amino acid solution.

Primary hepatocytes

Primary hepatocytes were isolated from C57BL/6 male mice at ~3–5 months of age as previously described[30] and plated in 6-well plates to ~85% confluency. Cells were allowed to adhere overnight, and all experiments were performed in William's Medium E (Gibco-Thermo Fisher Scientific, Waltham, MA, USA, Cat # A12176-01) supplemented with 10% FBS (unless serum starved), 1% antibiotic–antimycotic solution, and 1% L-glutamine.

Proliferation survival assays

Cells were seeded in 96-well plates at 3,000 cells/well and allowed to adhere overnight. Treatment with the indicated drug concentrations of Lenvatinib mesylate (Cayman Chemicals, Prod no:29832), and sodium salicylate (Millipore Sigma, Burlington, VT, USA, Cat # 567630) were applied to fresh media and incubated for 72 h (when control wells reached ~80% confluence). Cells were stained with Crystal Violet and analyzed as previously described.[28] The C_{max} for LEN in patients with HCC on an 8-mg LENVIMA® regimen is 68.3 ± 18.1 ng/ml, corresponding to 130.592 ± 34.608 nM,[31] justifying the *in vitro* doses used.

Clonogenic survival assay

Cells were seeded in 12-well plates at 1,000 cells/well and experiments were performed as previously described[28] using the indicated doses for 7days.

HSA model: Synergy Finder analysis

The highest single agent (HSA) Synergy Finder model quantifies the excess response (inhibition) over the highest single-drug response. Proliferation data expressed as % viability (control 100% survival) and individual experimental replicates were uploaded into Synergy Finder Web Tool (https://synergyfinder.fimm.fi/). Replicate data (n = 3 experimental replicates with n = 2 technical replicates each) were used and fitted by a four-parameter logistic curve for robust dose–response curve fitting; outlier detection was also utilized. Dose–response matrix analysis generated a heat map and synergy analysis yielded synergy scores (δ) for every individual drug combination depicted on the 3D heat map. Scores <-10, between -10 and 10 and >10 identified antagonistic, additive, or synergistic drug interactions respectively.

Fibrosis and tumors MASH model

Eight-week-old C57BL6/J male mice were housed in a specific pathogen-free facility in accordance with McMaster University Animal Ethics Research Board and subjected to CCl_4 (Sigma, Burlington, VT, USA, 289116-100 ML) and Western diet (Teklad Diets, 120528), also known as the fibrosis and tumors (FATMASH) model.[32] CCl_4 was delivered at a dose of 0.2 μl (0.32 μg)/g of body weight in corn oil and injected intraperitoneally once a week, starting simultaneously with diet administration. After 24 weeks of model development, mice were evenly divided into four groups; vehicle control, SAL (Cayman Chemicals, Product no: 11911) (300 mg/kg/day), LEN (Cayman Chemicals, Prod no: 29832) (2.5 mg/kg/day), and COMBO (300 and 2.5 mg/kg/day respectively). Drugs were administered via gavage 6 days per week for 6 weeks (experimental endpoint: 30 weeks).

Sample size calculations were based on data from Tsuchida *et al.*,[32] taking into considerations that all Western diet and CCl_4-treated mice would develop tumors and advanced MASH by 24 weeks. To achieve a meaningful effect size (0.5) with a SD (~0.2-0.5, for components of NAS), 80% power, and 5% significance level, a minimum of eight mice were required. Three additional mice per group were used to account for any premature deaths.

Tissue and serum collection

Mice received a single dose of ketamine/xylazine; once fully anesthetized, blood was collected via cardiac puncture, the liver was excised, and any tumors were resected. Sections of normal or tumoral tissues were fixed in 10% formalin or frozen for biochemical/molecular analysis. Tissues were weighed to identify tumor burden. Blood samples were placed in Eppendorf tubes and centrifuged at 10,000 rpm for 10 min at 4 °C, serum was stored at -80 °C.

Body composition

Body composition was analyzed using the Bruker's Minispec Whole Body Composition Analyzer (Bruker-LF90, Billerica, MA, USA) and its software.

Histological analysis

Tissues from the FAT-MASH model were fixed in 10% formalin for 48 h and subsequently placed in 70% ethanol. Following tissue processing and paraffin embedding, liver sections were stained with H&E, picrosirius red (PSR), or CD31/PCAM-1(CST #77699). CD31 staining was done with epitope retrieval, bond polymer refine detection (DS9800) using primary antibody diluted in power vision super blocker (PV6122) at a 1:100 dilution, using a Leica Bond RX automatic stainer. Ki67 (ab16667) and Cleaved caspase-3 (CST #9664) staining was performed using 1:150 and 1:400 dilutions, respectively.

PSR and CD31 quantification

Five photos per liver/per stain were taken using the Nikon Eclipse T3400 and NIS element D4.50.00 version 4.5 software. Quantification of stains was performed on ImageJ using standard color deconvolution. PSR and CD31 analyses were done using 8-bit (red channel) and HDAB color deconvolution (brown and blue) thresholding, respectively. Data were expressed as the % PSR, and % CD31 positive/Hematoxylin areas.

Histopathological evaluation and findings

NAS and fibrosis scoring

All histopathologic evaluations, including scoring, were performed in a blinded fashion by a pathologist. The nonalcoholic fatty liver disease activity score (NAS) and fibrosis score were determined as previously described.[30]

Neoplastic and non-neoplastic proliferative lesions. In the CCl_4 model, hepatic lesions were histologically identified as non-neoplastic proliferative lesions (slightly atypical hepatocytes with enlarged nuclei, higher nuclear:cytoplasm ratio, and basophilic or eosinophilic cytoplasm with preserved liver architecture) and neoplastic lesions (disorganized hepatic architecture comprising atypical hepatocytes with enlarged, pleomorphic, and occasional binucleated nuclei, irregular nuclear membrane, prominent nucleoli, cytoplasmic alterations, and balloon cells containing Mallory Denk bodies). Total number of lesions, number of non-neoplastic proliferative lesions, number of neoplastic lesions as well as percentage of parenchymal involvement by neoplasm and greatest diameter of largest tumor were evaluated on H&E-stained liver sections.

Quantification of neoplastic, non-neoplastic proliferative lesion area, and CC3 or Ki67 staining. All lesions and whole-liver sections were marked and annotated in the Qupath application by a pathologist and then quantified (μm^2). The percentage of liver involvement by each type of lesion was calculate by dividing the total lesion area by the whole-liver section. The same regions of interest (ROIs) were used to quantify the Ki67 or CC3 stain in the CCl_4 model using positive cell detection for DAB staining. Data were expressed as the percentage of positively stained cells per lesion type (neoplastic or non-neoplastic proliferating lesions).

Quantification of necrosis. Necrosis in excised xenograft tumors was assessed in the Qupath application by a pathologist. Briefly, the pixel classifier was trained by the pathologist to accurately distinguish between necrosis, tumor, blood, empty space, or other background staining. A 20x magnification was used to confirm the accuracy of the pixel classifier, and a ROI was applied to the entire excised tumor and necrotic area was quantified (expressed % necrosis relative to entire tumor). Fig. S1O provides a demonstration of the histological classification of necrosis by pixel classifier.

Type of steatosis. Microvesicular steatosis was reported as being either present or absent in non-tumoral liver tissue (non-neoplastic proliferative foci were excluded).[33] This was conducted by a pathologist using a 10x magnification, with 40x magnification for confirmation. Microvesicular steatosis was defined as the presence of non-zonal, contiguous patches of 'foamy hepatocytes with centrally placed nuclei' on H&E-stained slides. Macrovesicular steatosis (large droplet type) was identified as hepatocytes containing one large lipid droplet, pushing the nucleus to the periphery, whereas macrovesicular steatosis (small droplet type) was observed as hepatocytes filled with few large fat droplets with central nuclei (Fig. S3P).

Orthotopic Hep3B xenograft model

Three-month-old NRG mice were housed in a pathogen-free facility with *ad libitum* access to chow diet and water. All animal procedures were approved by the McMaster University Animal Ethics Research Board. Mice were prepared for orthotopic engraftment of Hep-3B-Luc-1 cells (luminescing). Surgical engraftment was performed as described,[34] and $1x10^{12}$ Hep-3B-Luc-1 cells in a 1:1 PBS:Matrigel mixture were injected directly into the lower left lobe of the liver. Mice were administered an additional carprofen dose (5 mg/kg) and allowed to recover on a heating pad for ~30 min. They were monitored daily for 7 days, followed by surgical clip removal. Engraftment was confirmed via In Vivo Imaging System (IVIS) imaging system (PerkinElmer, Waltham, MA, USA). Ten days post xenograft, mice were assigned, and treatment protocol was initiated. SAL was incorporated into standard chow diet at 2.5 g/kg diet for an average intake of 250 mg/kg/day. LEN was delivered via daily gavage of 2.5 mg/kg/day in VEH containing 0.5% carboxymethyl cellulose and 0.025% Tween-20, pH 7–8. Mice were continuously monitored until the survival endpoint was reached (body condition decline corresponding to profound weight loss [>20%], signs of extreme lethargy and/or reduced activity and grooming, development of ascites or jaundice and cachexia) in addition to luminescent signal monitoring.

Sample size calculations were based on preliminary tests in our laboratory. A minimum of eight mice was required for an

effect size (0.5) with a SD (~0.5, endpoint tumor size), 80% power and 5% significance level. A further two mice were added to account for an 80% success rate in tumor grafting.

AFP quantification by ELISA

Circulating levels of alpha fetoprotein (AFP), an HCC biomarker,[35] were analyzed in the serum of mice from the FATMASH model collected at end point (30 weeks). Mouse AFP measurements were performed using a DuoSet ELISA kit (R&D Systems, Cat # DY5369-05) following the manufacturer's instructions. Serum samples were diluted (1:150–1:500) in mice with no histological indication of tumors and (1:2,000–1:8,000) for mice in which dysplastic nodules or neoplastic nodules were observed.

Protein immunoblotting

Cells were homogenized in lysis buffer.[28] Sample preparation, electrophoresis, wet transfer, and imaging were performed as previously described.[28] A total of 12 μg of protein from each sample alongside Precision Plus Protein Dual Color Standard (Bio-Rad, Hercules, CA, USA) were run. Primary anti-rabbit antibodies and the secondary antibody were diluted at 1:1,000 and 1:10,000 dilution respectively (Cell Signalling Technologies, Danvers, USA; see the Supplementary CTAT table for details).

De novo lipogenesis assay

Primary mouse hepatocytes were isolated and seeded in 12-well plates. The next day, a 2-h serum starve followed by the treatment with indicated drugs (VEH, SAL 1 mM, LEN 0.1 μM, or COMBO) in the presence of ^{14}C-acetate (1 μCi/ml) was performed. Acetic acid, sodium salt labeled at the 1 position with ^{14}C (Perkin Elmer, Cat # NEC084A001MC) and cold sodium acetate (Sigma, cat # S2889-250G) were used. After 4 h of treatment, plates were washed three times in 1x PBS, scraped in 100 μl of PBS, mixed with 300 μl of 2:1 chloroform:methanol and then vortexed. Next, 100 μl of H_2O was added and the cells were vortexed again and centrifuged at 18,000 rpm at room temperature for 5 min. The bottom layer was extracted and added to 5 ml of scintillation fluid for 30 min to determine ^{14}C incorporation into lipids.

Fatty acid oxidation assay

FAO was performed by measuring the amount of [C^{14}]-palmitate contained in the bicarbonate pool (CO_2 fraction) and from citric acid cycle intermediates (acid-soluble material; ASM). First, cells were serum starved for 2 h in William's E Medium (WME). Next, they were pretreated with drug-supplemented WME, which included VEH (DMSO 1:1,000 dilution), SAL (1 mM), LEN (0.1 μM) or COMBO with cold palmitate (0.5 mM) (Sigma, Cat # P9767-5G) and L-carnitine hydrochloride (1 mM) for 30min. Media were removed and refreshed with the same media also containing [C^{14}]-palmitate (0.5 μCi/ml) for 3 h (Perkin Elmer, Cat # NEC075H250UC).

To liberate the CO_2 produced, 2 ml of media was added to a glass scintillation vial containing 2 ml acetic acid (1 M) and sealed immediately. To trap the CO_2, these vials also contained 450 μl of benzethonium hydroxide in 0.5-ml Eppendorf tubes sitting within a 1.5-ml tube. Samples were then placed on an orbital shaker for 2 h at 75 rpm. After incubation, the inner tube containing benzethonium hydroxide was removed and transferred to a plastic scintillation vial, where 5 ml of scintillation fluid (Ultima Gold) (Sigma, Cat # L8286) was added.

For the ASM fraction, cells were scraped on ice in 200 μl of PBS and transferred to an Eppendorf tube. Next 750 μl of chloroform:methanol (2:1) was added followed by a 15-s vortex and rest at -20 °C for 10 min. Next, 250 μl of chloroform and 250 μl of H_2O were added and samples were inverted and centrifuged at 3,000 rpm for 10 min at 4 °C. The aqueous phase was then transferred to a plastic scintillation vial, followed by the addition of scintillation fluid (5 ml). Both ASM and CO_2 fractions were mixed by inversion and allowed to quench overnight in the dark before scintillation counting the following day. Counts were measured in disintegrations per minute (DPMs), and data are presented as the sum of DPMs from both the ASM and CO_2 fractions.

Cell cycle flow cytometry

Hep3B cells were seeded in 10-cm dishes at 350,000 cells/dish and allowed to adhere overnight in complete media (DMEM + 10% FBS + 1% AA). Following 24-h complete serum deprivation, cells were washed with PBS and placed in media containing 5% serum in addition to drug treatments (VEH-DMSO, SAL 1 mM, LEN 100 nM or COMBO) for 24h. Cells were fixed using ethanol and analyzed using flow cytometry as previously described.[36]

RNA isolation

RNA was isolated from cells or liver tissue using TRIzol™ (Life Technologies, Grand Island, NE, USA) and purified using RNeasy kit (QIAGEN, Germantown, MD, USA Cat # 74106) as previously described.[30]

RNA-sequencing pipeline

All RNA-sequencing data are available using GEO accession number GSE282660.

Hep3B cells

RNA sample quality was first assessed using Agilent 2100 Bioanalyzer G2938C with the Agilent RNA6000 Nano Kit (Agilent, Santa Clara, CA, USA). Next, the NEBNext Poly(A) mRNA Isolation Module (NEB, Ipswich, MA, USA) was used for mRNA enrichment, followed by an NEBNext® Ultra™ II Directional RNA library kit (NEB) for library preparation. Illumina HiSeq1500 (Illumina; San Diego, CA, USA) next-generation sequencing was performed at the McMaster Genomics Facility with HiSeq Rapid version 2 flow cells to eliminate lane-specific effects. Paired-end sequencing yielded 400 million clusters (~22 million per sample). Raw fastq data were uploaded to the opensource platform Galaxy (usegalaxy.org) for quality control and processing. Owing to data corruption, only R1 files were used, and the dataset was treated as single-end, with corrupted R2 files excluded. FastQC was used to evaluate read quality before and after adaptor trimming and low-quality read removal using Cutadapt. High-quality reads were aligned to the human hg38 reference genome using HISAT2, and aligned reads were quantified with featureCount. Differential expression analysis

between experimental conditions was performed using DESeq2.

FAT-MASH mouse livers

RNA sample quality, mRNA enrichment, and library preparation were performed following the same procedure as for Hep3B cells. Sequencing was performed at the McMaster Genomics Facility (with a NextSeq 2000 instrument; P2, 2x50 bp). Raw fastq data were uploaded to the opensource platform Galaxy (usegalaxy.org) for quality control and processing. FastQC was used to evaluate read quality before and after adaptor trimming and low-quality read removal using Cutadapt. High-quality reads were aligned to the murine mm10 reference genome using HISAT2, and aligned reads were quantified with featureCounts. Counts data were exported to R for differential expression analysis with the DESeq2 package to detect significant differentially expressed genes (DEGs) (p-adj <0.05).

Analysis of bulk RNA data

Venn diagrams were generated using the *ggVennDiagram* R package to compare the DEGs in each treatment condition (relative to control). Gene set enrichment analysis (GSEA) was performed using ranked files generated from DESeq2 output. Genes were ranked by p-adj, with downregulated genes given negative rank scores and upregulated genes positive rank scores. Hallmark and Gene Ontology Biological Process (GOBP) gene sets were downloaded from MSigDB (www.gsea-msigdb.org/gsea/msigdb/). The SimplifyEnrichment R package was used to remove redundant GOBP pathways for these visualizations.

Liver cell type analysis using the Azairani Dataset (www.gsea-msigdb.org/gsea/msigdb/human/genesets.jsp?collection=C8) was performed using GSEA and single-sample gene set enrichment analysis (ssGSEA). Gene sets were mouse genes orthologous to the human liver gene sets curated by Azairani *et al.* (https://www.gsea-msigdb.org/gsea/msigdb/human/genesets.jsp?collection=C8). Heatmaps were generated using Morpheus (Broad Institute, Cambridge, MA, USA). Genes included in heatmaps were extracted from select gene sets.

iRegulon *in silico* transcriptional regulator analysis software reverse engineers the transcriptional regulatory network underlying a co-expressed gene set using *cis*-regulatory sequence analysis. The software then scores the top up- or downregulated regulons (transcription factors and co-factors) based on a normalized enrichment score (NES). Only statistically significant genes (p-adj ≤0.05) were used for the indicated comparison.

Results

Salsalate plus lenvatinib treatment suppresses human HCC cell growth and improves survival in mice with orthotopic xenografts

To examine the direct tumor effects of SAL and LEN, we performed proliferation assays on the human HCC cell line Hep3B (containing mutant *TP53*, *AXIN1*, and *RB1*) and found that LEN (IC_{50} ~1.58 μM) and SAL (IC_{50} ~2.76 mM) both inhibited proliferation (Fig. 1A; Fig. S1D). Similar inhibition of proliferation survival was observed for SAL and LEN in HepG2 (*TERT*, *NRAS*, and *CTNNB1* mutant) hepatoblastoma cells as well as PLC/PRF/5 (*TP53*, *CDKN2A*, *TSC2*, and *AXIN1* mutant) and Huh7 (*TP53*, *TERT*, *KDR*, and *POLD3* mutant) HCC cell lines (Figs. S1A–D). Drug synergy was assessed using a proliferation assay dose matrix of single agent and COMBO treatments and showed a consistent enhancement of the antiproliferative activity of both SAL and LEN over a range of COMBO doses (Fig. 1B). These data were analyzed with the HSA synergy score model (see Materials and Methods) and demonstrated significant synergy between SAL and LEN (Fig. 1C). In particular, clinically achievable COMBO treatments[14,31,37] comprising SAL at 0.5 mM paired with LEN at 0.05 μM, or SAL at 1 mM paired with LEN at 0.1 μM (Table S1) were highly synergistic. Of note, all drug combinations tested suppressed cell proliferation in either an additive or synergistic manner and were not antagonistic (Table S1). Specifically, SAL at 1 mM paired with LEN at 0.1 μM showed significant suppression of cell proliferation (Fig. 1D), while clonogenic survival, a metric of cancer cell oncogenic potential, was inhibited by >95% (Fig. 1E). COMBO treatment also led to greater inhibition of clonogenic survival compared with SAL or LEN monotherapy in HepG2, PLC/PRF/5, and Huh7 cell lines (Figs. S1E–G).

To determine whether COMBO therapy might also reduce tumor growth *in vivo*, we conducted a survival analysis in which luciferase-expressing Hep3B cells were surgically engrafted into the livers of NRG mice. After confirmation of Hep3B engraftment (Table S2), mice were treated with vehicle (VEH), LEN 2.5 mg/kg, SAL 300 mg/kg, or COMBO. The endpoint was primarily determined based on body condition comprising body-weight loss, signs of cachexia, lethargy, dehydration, and a luciferase signal of ~$1x10^6$ p/s/cm^2/sr (Table S2). Kaplan–Meier survival analysis revealed that, while LEN and SAL showed trends for improved survival (~58% and ~54%, respectively, p >0.05) only the COMBO therapy significantly increased survival (~73%, p = 0.02) (Fig. 1F). The 90-day survival was 14%, 42.8%, 50%, and 71.4% for the VEH, SAL, LEN, and COMBO groups, respectively (Fig. 1G), indicating an approximately threefold increase in survival for monotherapies compared with VEH and an approximately fivefold increase for COMBO therapy (Fig. 1G). Body weight throughout the experiment (Fig. S1I), as well as endpoint liver mass, following tumor excision (Fig. S1J) and total tumor burden (Table S2 and Figs. S1h and k), were similar between groups at endpoint. There were no differences in quantification of necrosis (see Methods) (Fig. S1L) or apoptosis marker (cleaved caspase 3, CC3, Fig. S1M) among treatments. However, the proliferation marker (Ki67) was reduced by SAL and LEN compared with VEH (Fig. S1N). These data indicate that, consistent with reductions in proliferation and clonogenic survival observed in cultured Hep3B cells, COMBO therapy also improved survival when these cells were engrafted in the livers of NRG mice.

Salsalate plus lenvatinib mediates substantial transcriptional reprograming in HCC cells

To better understand the mechanisms contributing to the antitumor efficacy of LEN, SAL, and COMBO therapies, we conducted RNA-sequencing (RNA-seq) analysis in Hep3B cells (Fig. 2). LEN and SAL significantly increased 1,053 and 1,449

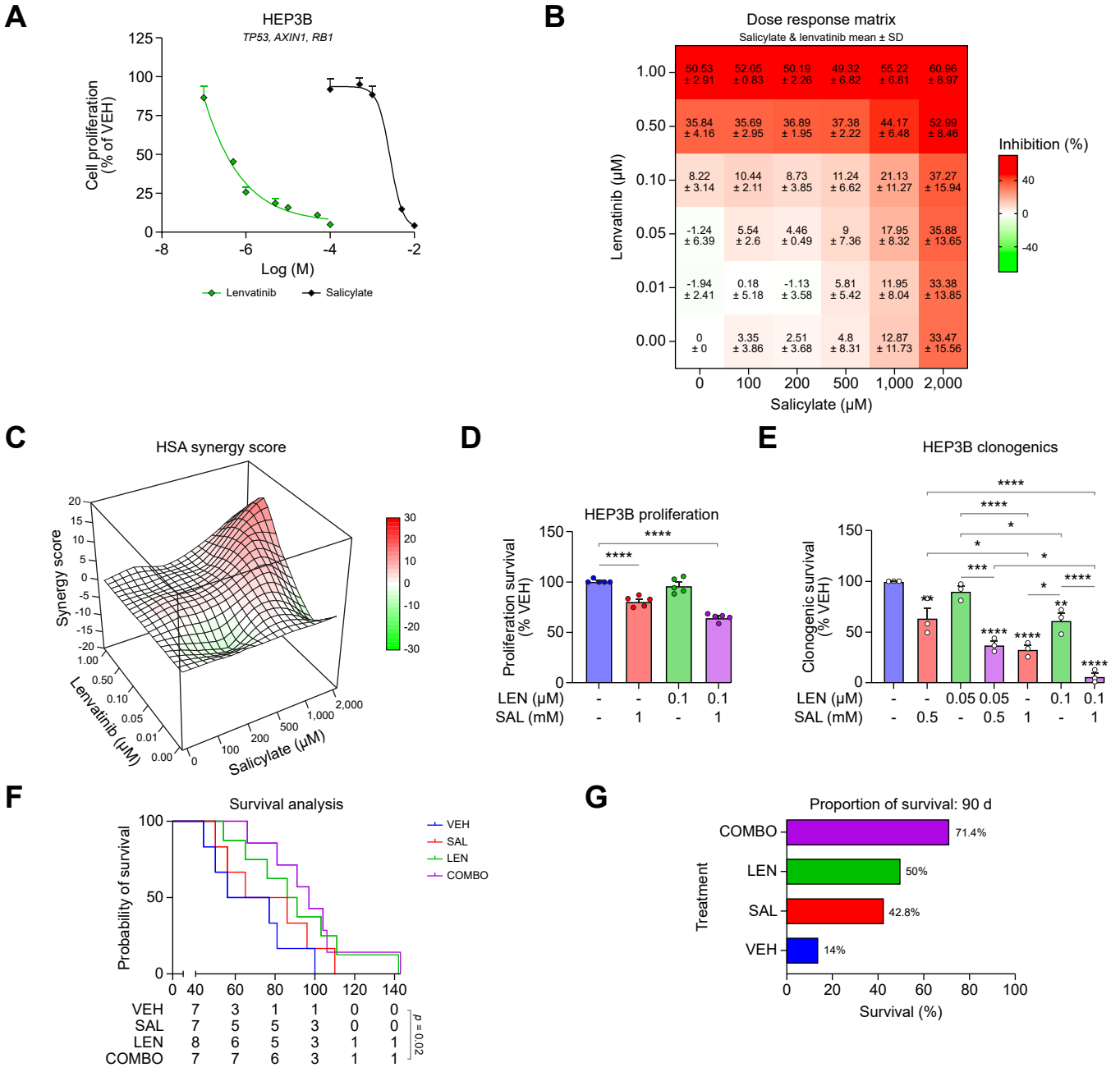

Fig. 1. Salicylate and Lenvantinib synergistically suppress growth and tumorigenic potential of HCC cells and improve survival in Hep3B xenografts. (A) 72-h proliferation dose response in cultured Hep3B cells following treatment with salicylate and lenvantinib and (B) dose–response matrix in cultured Hep3B cells treated with indicated doses of salicylate and lenvantinib. (C) HSA synergy score (δ) analysis plots for salicylate and lenvantinib COMBO dose–response matrix, (D) 72-h proliferation, and (E) 7-day Hep3B clonogenic assay in response to indicated doses of salicylate, lenvantinib or salicylate+lenvantinib. (F) Survival analysis of mice engrafted with Hep3B cells and treated with vehicle, (VEH), salsalate (SAL), lenvantinib (LEN) or salsalate+lenvantinib (COMBO) and (G) proportion of mice surviving 90 days after xenografts. Data are mean ± SD (B) and mean ± SEM (A,D,E) with N = 3, n = 6 (A–C), N = 5, n = 6 (D), and N = 3, n = 3 (E), HSA analysis to determine synergy (B,C) and one-way ANOVA with Tukey's multiple comparisons (D,E). n = 7, for VEH, SAL and COMBO groups and n = 8 for LEN treatments analyzed using a Log-rank (Mantel-Cox) test for comparison of survival curves (F); **p* ≤0.05, ***p* ≤0.01, ****p* ≤0.001, *****p* ≤0.0001. HAS, highest single agent; HCC, hepatocellular carcinoma; LEN, lenvatinib; SAL, salsalate.

DEGs and inhibited 1,215 and 1,679 DEGs, respectively, compared with controls. The COMBO therapy resulted in an increase in the number of DEGs, with 2,838 upregulated and 3,205 downregulated, compared to VEH (Fig. 2A). Remarkably, 17% of the significantly upregulated and 19% of significantly downregulated DEGs were unique to the COMBO therapy (red arrows in Fig. 2B).

GSEA revealed that, in response to COMBO treatment, key upregulated pathways included fatty acid catabolic processes and apoptotic signaling gene sets, while those encoding small and large ribosomes, ribosomal–RNA processes and fibroblast migration were suppressed (Fig. 2C). Many of these pathways overlapped with those targeted by SAL or LEN (Fig. S2). Further interrogation revealed that COMBO therapy

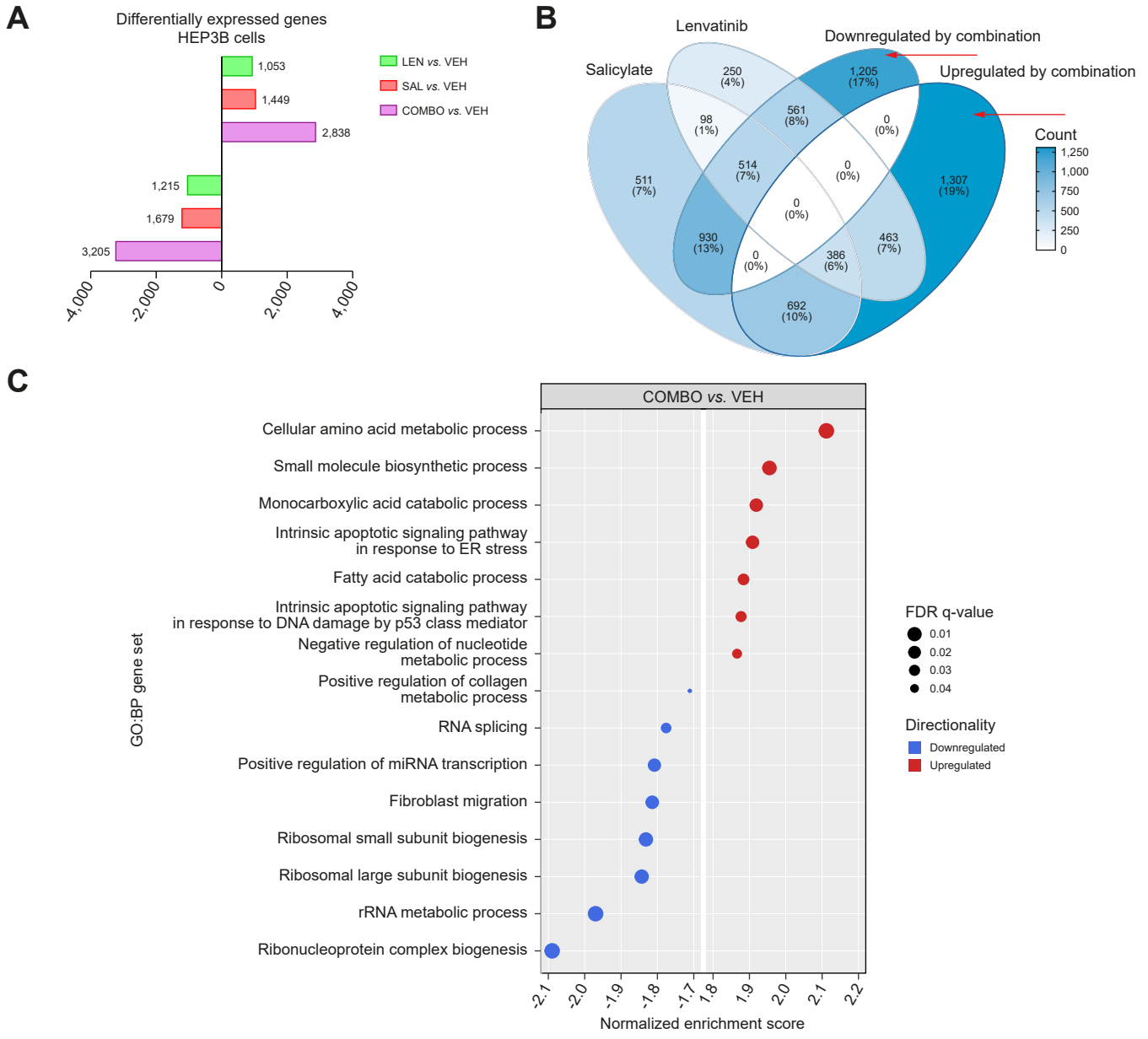

Fig. 2. COMBO therapy alters expression of key cancer growth-associated pathways in Hep3B cells. Bulk RNA-sequencing was performed in Hep3B cells treated for 9 h with LEN (100 nM), SAL (1 mM) or COMBO. (A) Number of up- or downregulated DEGS for each treatment comparison. (B) Number of DEGs altered by each single drug or COMBO; red arrows indicate upregulated or downregulated genes uniquely altered by COMBO. (C) Gene sets significantly changed in response to COMBO *vs.* VEH. All DEGs have an FDR q-value ≤0.05 (A,B), select significantly up- and downregulated gene terms have an FDR q-value ≤0.05 (C); n =3 technical replicates analyzed for each treatment condition. COMBO, lenvatinib + salsalate; DEG, differentially expressed gene; LEN, lenvatinib; SAL, salsalate; VEH, vehicle.

reduced DEGs associated with anaerobic glycolysis, while increasing DEGs associated with FAO/β-oxidation (Fig. 3A). Specifically, glycolytic genes, such as those encoding hexokinase (*HK2*), phosphoglycerate kinase (*PGK1*), pyruvate kinase (*PKM*), and lactate dehydrogenase (*LDHA*), were suppressed (*p*-adj ≤0.01), while those encoding key enzymes for FAO/β-oxidation, including long-chain acetyl-CoA synthetases (*ACSL1*, *ACSL3*, and *ACSL4*), carnitine palmitoyl transferases (*CPT1A* and *CPT2*), acyl-CoA dehydrogenases (*ACADS* and *ACADSB*), and hydroxyacyl-CoA dehydrogenase (*HADH*), were upregulated (*p*-adj ≤0.01) (Fig. 3A). The peroxisomal β-oxidation genes acyl-CoA oxidase 1 (*ACOX1*) and enoyl-CoA hydratase and 3-hydroxyacyl-CoA dehydrogenase (*EHHADH*) were also significantly upregulated. This increase in DEGs associated with increased β-oxidation coincided with the reciprocal inhibition of ATP citrate lyase (ACLY), a key enzyme controlling DNL.

In addition to metabolic reprogramming, there were changes in many transcriptional regulators, including an increase in the transcriptional co-activator PPARGC1A (*PGC1a*), which is critical for increasing oxidative metabolism and mitochondrial biogenesis (Fig. 3B). In contrast to *PGC1a*, other genes associated with transcription initiation, such as polymerases (POLR3H/2D/1E/1F/MT), elongases (ELOA/C), mediator

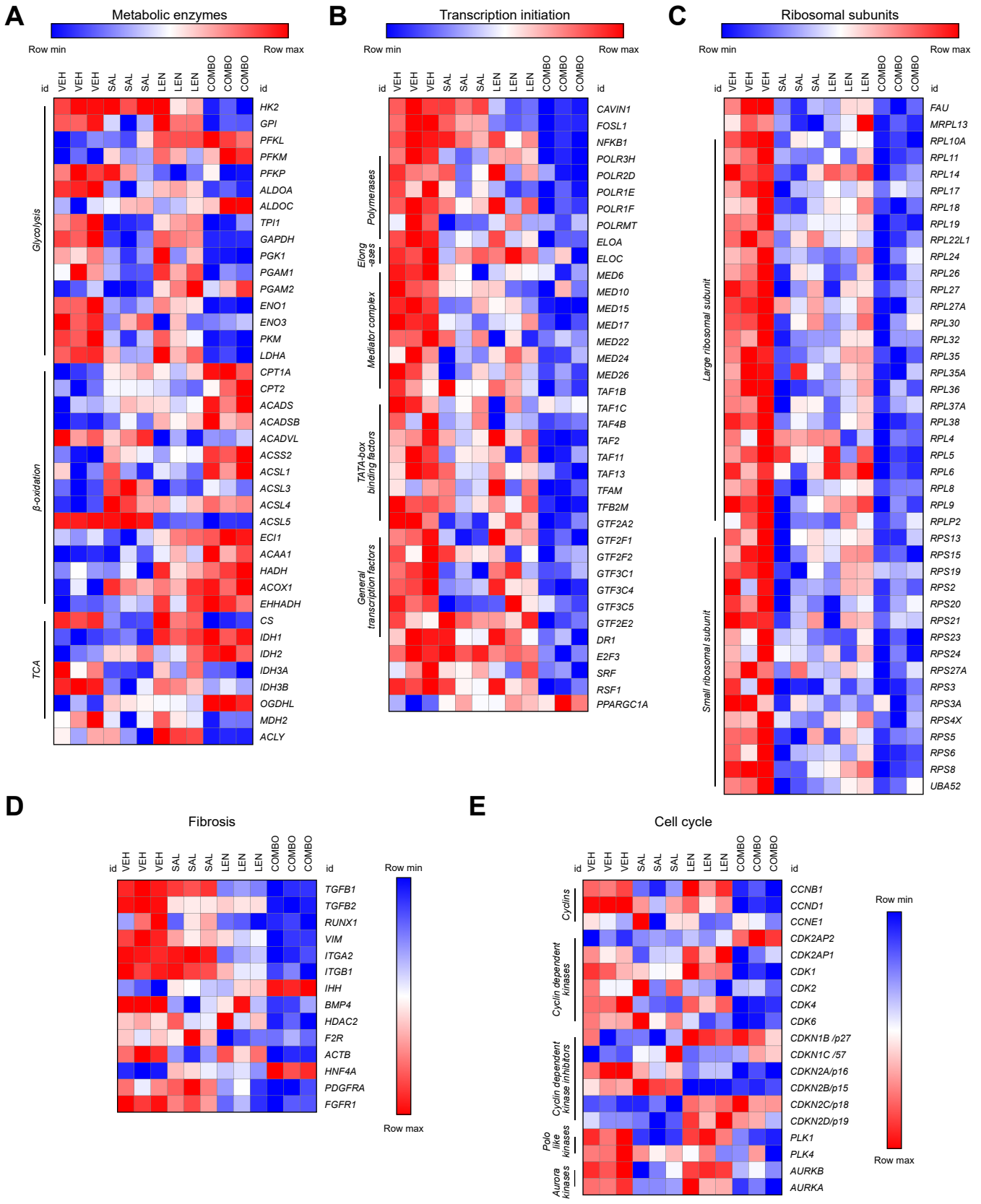

Fig. 3. COMBO therapy suppresses glycolytic metabolism, biosynthetic processes, and profibrotic signaling while increasing fatty acid oxidation and cell cycle regulation in HCC cells. Significantly differentially regulated genes in response to COMBO treatment (FDR q-value ≤0.05) for (A) metabolic enzymes, (B) transcriptional initiation, (C) genes encoding ribosomal subunits, (D) profibrotic signaling, and (E) cell cycle regulation; n = 3 technical replicates for each treatment condition. COMBO, lenvatinib + salsalate; FDR, false discovery rate; HCC, hepatocellular carcinoma.

complex subunits (MED6/10/15/17/22/24/26), TATA-box binding protein-associated factors (TAF1B, TAF1C, TAF4B, TAF2/11/13, and TAFB2M) and general transcription factors (GTF2A1/F1/F2, GTF3C1/C4/C5, and GTF2E2) were suppressed (p-adj ≤0.01) (Fig. 3B). We also observed broad suppression of genes encoding small and large ribosomal subunits in response to COMBO treatment (Fig. 3C).

COMBO therapy also mediated the suppression of genes associated with fibroblast growth factor signaling and collagen metabolism, such as transforming growth factor beta 1 (*TGFB1*), RUNX family transcription factor 1 (*RUNX1*), vimentin (*VIM*), and integrin subunit alpha 2 (*ITGA2*) (Fig. 3D). Genes mediating cell cycle progression, such as cyclins (B1, D1, and E1) and cyclin-dependent kinases (1, 2, 4, and 6) were significantly reduced, alongside Polo-like kinases and Aurora Kinases (p-adj ≤0.01), which are mediators of cell division[38–40] (Fig. 3E).

These data indicate that COMBO therapy with LEN and SAL in Hep3B cells exerts unique effects on the expression of transcripts important for controlling glycolysis, FAO/β-oxidation, transcription and ribosomal initiation factors, fibrosis, and cell cycle progression. Such processes are consistent with reduced proliferation and clonogenic survival.

Modulation of cellular signaling events

HCC tumors are characterized by increased aerobic glycolysis and DNL, and low rates of FAO.[6] Consistent with transcriptional changes detected from the RNA-seq analysis (Fig. 3A), SAL and COMBO therapy suppressed DNL (-48% and -68%, p ≤0.0001, respectively; Fig. 4A) and increased FAO (+45% and +57%, p ≤0.0001, Fig. 4B) compared with VEH or LEN. AMPK inhibits DNL and increases FAO through phosphorylation and inhibition of acetyl-CoA carboxylase (ACC).[25] Compared with VEH and LEN, both SAL and COMBO increased phosphorylation of ACC Ser79 (Fig. 4C). AMPK also inhibits proliferation by inhibition of mTORC1 targets. SAL and COMBO therapy increased Ser792 phosphorylation on Raptor (an AMPK phosphorylation site that inhibits mTOR activity) (Fig. 4D,E), and decreased phosphorylation of downstream mTORC1 substrates, p70 S6-kinase ($p70^{S6k}$) at Thr389 and ribosomal protein S6 phosphorylation at Ser240-244 (p-S6) (Fig. 4D,F,G). mTOR controls the expression of hypoxia inducible factor α (HIF1α), a key factor driving tumor angiogenesis and survival in the hypoxic tumor microenvironment.[41] Both SAL and COMBO dramatically reduced HIF1α (Fig. 4H). LEN reduces tyrosine kinase/growth factor signaling and we found that ERK1/2 phosphorylation at Thr202/Tyr204 was reduced by LEN and COMBO (Fig. 4I). In addition to these changes in cellular signaling, COMBO treatment induced an ∼20% reduction in cells distributed to the G2/M phase (Fig. 4J).

These data indicate that, consistent with reductions in cell proliferation and RNA-seq analysis, COMBO therapy increases FAO and reduces DNL, causes post-translational modifications on ERK and AMPK substrates ACC and mTOR, while reducing the protein expression of HIF1α and cells entering G2/M phase.

Mouse liver and tumors are comprised primarily of an AMPKα1β1γ1 heterotrimer and genetic deletion of AMPKβ1 results in nearly undetectable AMPK activity.[42,43] To assess the importance of AMPKβ1 in mediating the antiproliferative effects of LEN and SAL, we conducted experiments in MEFs from wild-type (WT) and AMPKβ1-knockout (KO) mice; AMPKβ1 KO removes nearly all detectable AMPK activity, similar to the hepatocytes of AMPKβ1-null mice.[42] We then compared these findings to the AMPKβ1-selective small-molecule AMPK activator PF-06409577.[44] LEN exerted a similar reduction in proliferation in both WT and AMPKβ1 KO MEFs, indicating that AMPKβ1 was not required (Fig. 4K). By contrast, the effects of both SAL (Fig. 4L) and PF-06409577 (Fig. 4M) on proliferation were blunted in the absence of AMPKβ1. Importantly, the combination of LEN with PF-06409577 restricted proliferation in an additive manner (Fig. 4N), similar to that observed with COMBO (Fig. 1D). These data suggest that AMPKβ1 is important for some of the antiproliferative actions of SAL and that other pathways are also involved.

Salsalate and lenvatinib reduce liver steatosis, fibrosis, and angiogenesis

Fibrosis, inflammation, and angiogenesis are important drivers of MASH-related HCC that contribute to therapy resistance.[45] To examine whether COMBO also exerts positive effects on the liver microenvironment, we conducted studies with a metabolic carcinogenesis mouse model. Mice were fed a Western diet (high fat, cholesterol, and sugar [fructose and glucose]) in combination with weekly intraperitoneal CCl_4 injections stimulating liver fibrosis and carcinogenesis (FAT-MASH) as previously described[32] (Fig. 5A).

After 24 weeks, FAT-MASH mice were randomly allocated to receive VEH, LEN, SAL, or COMBO therapy for 6 weeks. There were no significant differences in body weight, food intake, or body composition at any point throughout the treatment period in any group compared with VEH (Figs. S3A–D). At 30 weeks, livers were collected and fixed. Excised liver weights in all treatment groups were similar to VEH (Fig. S3E). In contrast to previous descriptions of the model,[32] circulating levels of AFP were elevated in only two animals within the VEH group and four animals in the LEN group suggesting significant heterogeneity and low tumor burden in the VEH group (Fig. S3F). Consistent with AFP, the total number of lesions (Fig. S3G) and tumor burden (neoplastic lesion number and involvement [% total liver area]) was low in all treatment groups (Figs. S3H and I). Quantification of non-neoplastic proliferative lesion involvement also showed no difference between groups (Fig. S3J). Similarly, immunohistochemical analysis of proliferation and apoptosis markers (Ki67 and CC3, respectively) revealed no meaningful trends (Fig. S3K–P). Thus, a lower tumor burden in this model precluded assessment of the effects of combination therapy on HCC.

The FAT-MASH model is considered one of the best preclinical models of MASH and fibrosis, key drivers of HCC.[46] Histological assessment of inflammation, ballooning, and steatosis, performed to determine the NAS (a combined score of inflammation, ballooning, and steatosis) on H&E-stained livers, indicated significant MASH in VEH controls (Fig. 5B–G). Although treatments had no significant effects on inflammation (Fig. 5D) or ballooning scores (Fig. 5E), COMBO reduced steatosis scores (Fig. 5F) and the composite NAS (Fig. 5G). Analysis of macrovesicular and microvesicular steatosis (see Fig. S3P for pathological description) revealed a tendency for reductions in macrovesicular steatosis with COMBO (p = 0.078) and microvesicular steatosis in response to SAL (p = 0.058) and COMBO (p = 0.056) (Fig. 5H,I). There was reduced expression of the endothelial cell marker CD31 in LEN and COMBO compared with VEH or SAL treatment groups (Fig. 5J,K),

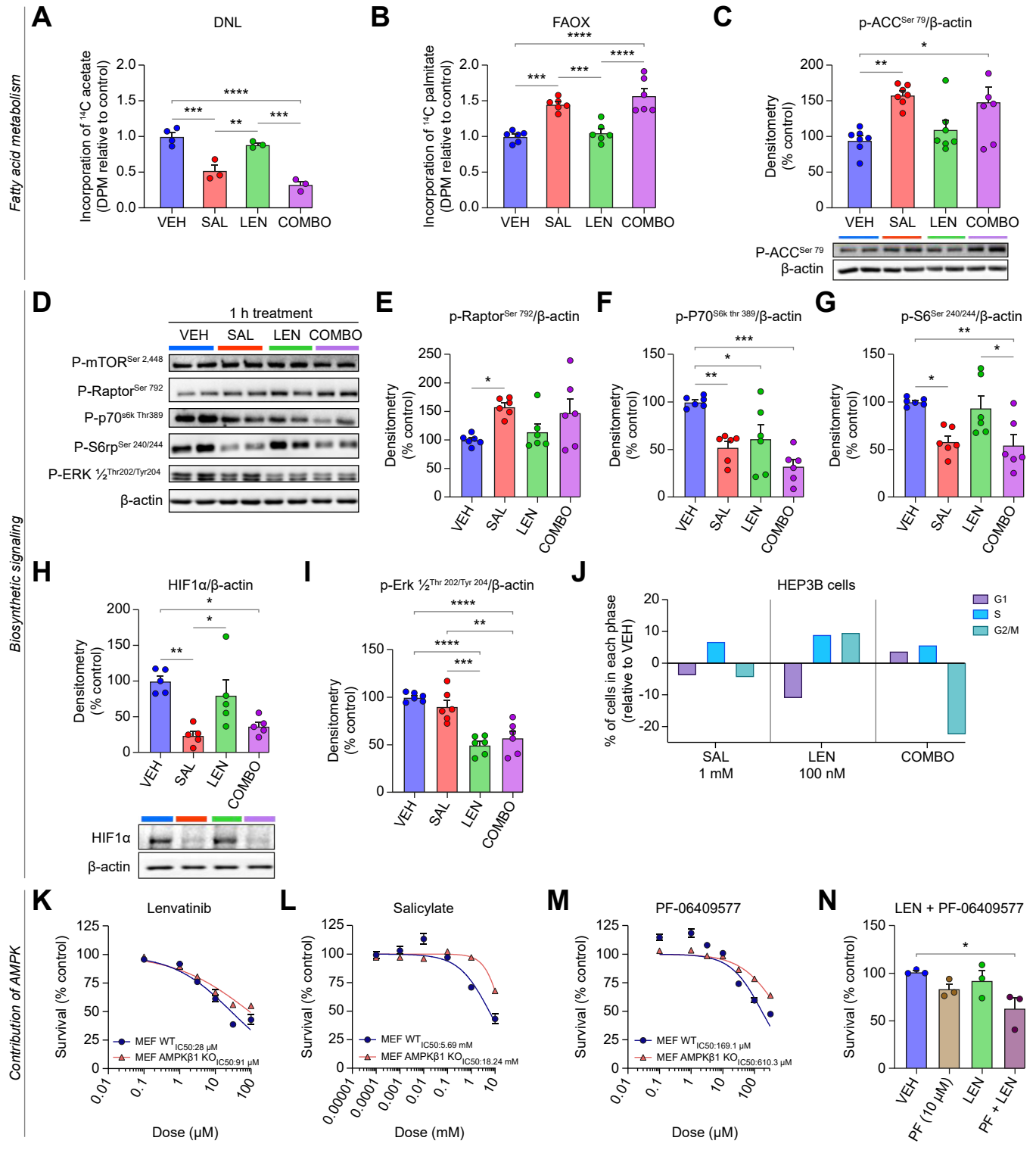

Fig. 4. COMBO therapy increases AMPK and fatty acid oxidation while suppressing lipogenesis, HIF1a, ERK and mTOR. [C^{14}]-acetate and [C^{14}]-palmitate were used to analyze (A) DNL and (B) FAO, respectively. (C) Immunoblotting for p-ACC evaluated in response to 1-h treatment of standard dosing (VEH [DMSO], SAL [1 mM], LEN ([100 nM] or COMBO). (D) Representative blots for phosphorylated proteins in response to 1-h treatment; resulting quantification for (E) p-Raptor, (F) p-p70, and (G) p-S6 (G). Immunoblotting for (H) total HIF1α levels in response to 24-h treatment and standard treatment doses and (I) p-ERK in response to 1-h treatment. (J) Cell cycle phase distribution compared with VEH. Proliferative survival in response to (K) LEN, (L) SAL, or (M) the AMPKβ1 activator PF-06409577 in WT or AMPKβ1-KO MEFs. (N) Proliferation response in Hep3B cells treated with PF-06409577 (10 μM), LEN (100 nM) or COMBO. Data are presented as mean ± SE; IC_{50} determined using nonlinear regression of (inhibitor *vs.* normalized response) (K–M); data analyzed with one-way ANOVA with Tukey multiple comparisons (A–C,E–I,N) or chi-square tests (J); **p* ≤0.05, ***p* ≤0.01, ****p* ≤0.001, *****p* ≤0.0001; n = 3 and n = 6 technical replicates used to generate (A) DNL and (B) FAO data, respectively. Western blot data comprise n = 3 experimental and n = 2 technical replicates (C,E–I), 10,000 events for cell cycle distribution analysis (J), and N = 3 experiments with n = 6 technical replicates each for proliferation response (K–N). ACC, acetyl-CoA carboxylase; AMPKβ1, AMP-activated protein kinase β1; COMBO, lenvatinib + salsalate; DNL, *de novo* lipogenesis; FAO, fatty acid oxidation; HIF1α, hypoxia inducible factor alpha; KO, knockout; LEN, lenvatinib; SAL, salsalate; VEH, vehicle; WT, wild-type.

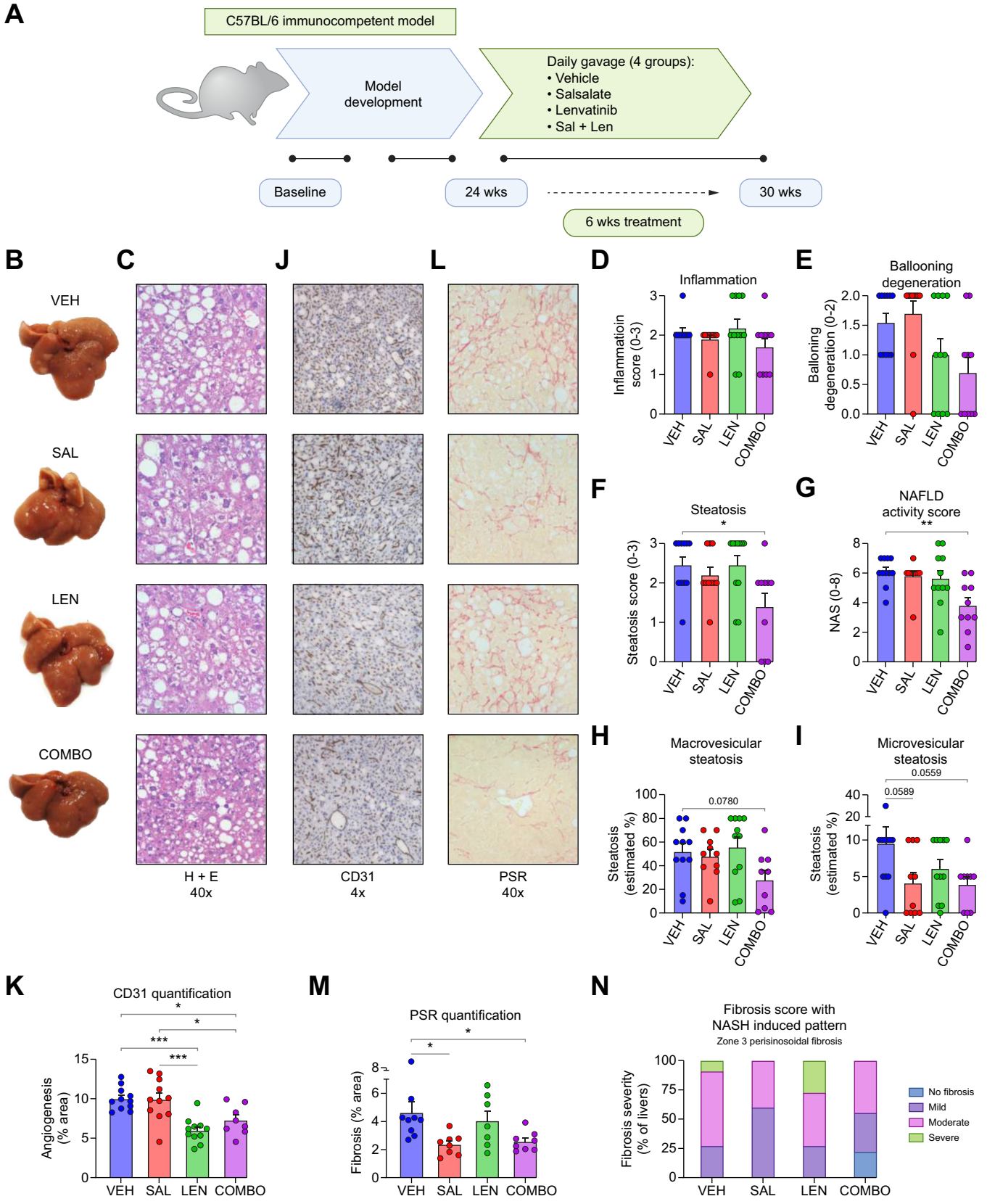

Fig. 5. SAL and COMBO tend to reduce NAS, angiogenesis, and fibrosis in the FAT-MASH mouse model. (A) Model design, (B) representative whole-liver photo, (C) H&E liver images, analyzed for NAS variables, (D) inflammation, (E) ballooning degeneration, (F) steatosis, (G) composite NAS, and (H) macrovesicular or (I) microvesicular steatosis. (J) CD31 stain and (K) digital quantification. (L) PSR stain and (M) digital quantification alongside (N) pathological fibrosis score. Data are presented as mean ± SEM, analyzed by one-way ANOVA with Tukey multiple comparisons; *$p \leq 0.05$, **$p \leq 0.01$, ***$p \leq 0.001$, based on eight or more mice per group; analysis for each mouse liver was generated from five digitally quantified images per liver (D–N). (A) created using BioRender (biorender.com). COMBO, lenvatinib + salsalate; NAS, nonalcoholic fatty liver disease activity score; PSR, Picrosirius Red; SAL, salsalate.

highlighting the anti-angiogenic action of LEN. Importantly, liver fibrosis (% PSR-positive area) and fibrosis severity (proportion of livers with severe fibrosis) were reduced in the SAL and COMBO groups compared with VEH (Fig. 5L–N). These data indicate that, in the FAT-MASH model, COMBO reduced steatosis, NAS, and markers of fibrosis and angiogenesis.

Salsalate and lenvatinib combination therapy elicits transcriptional control of fatty acid oxidation and angiogenesis in mouse livers *in vivo*

To examine mechanisms for the reduced steatosis, angiogenesis, and fibrosis in the FAT-MASH model, we conducted RNA-seq of the livers of mice treated with VEH, SAL, LEN, or COMBO described above. Similar to observations in Hep3B cells, COMBO led to a greater number of DEGs compared with monotherapies (Fig. 6A) and uniquely upregulated 31% and downregulated 25% of these DEGs (Fig. 6B). GSEA analysis indicated that COMBO upregulated FAO/β-oxidation and mitochondrial gene expression, whereas gene sets associated with angiogenesis and immune responses were downregulated (Fig. 6C). Furthermore, the upregulation of FAO gene sets appeared to be largely driven by SAL (Fig. 7A; Fig. S4A). As anticipated, the reduction in angiogenesis was primarily mediated by LEN (Fig. 7B; Fig. S4B) with significant reductions in the COMBO group in important transcripts, including delta-like canonical notch ligand 4 (*Dll4*), vascular endothelial growth factor receptor 2 (*Vegfr2/Kdr*), angiopoietin 1 and 2 (*Angpt1* and

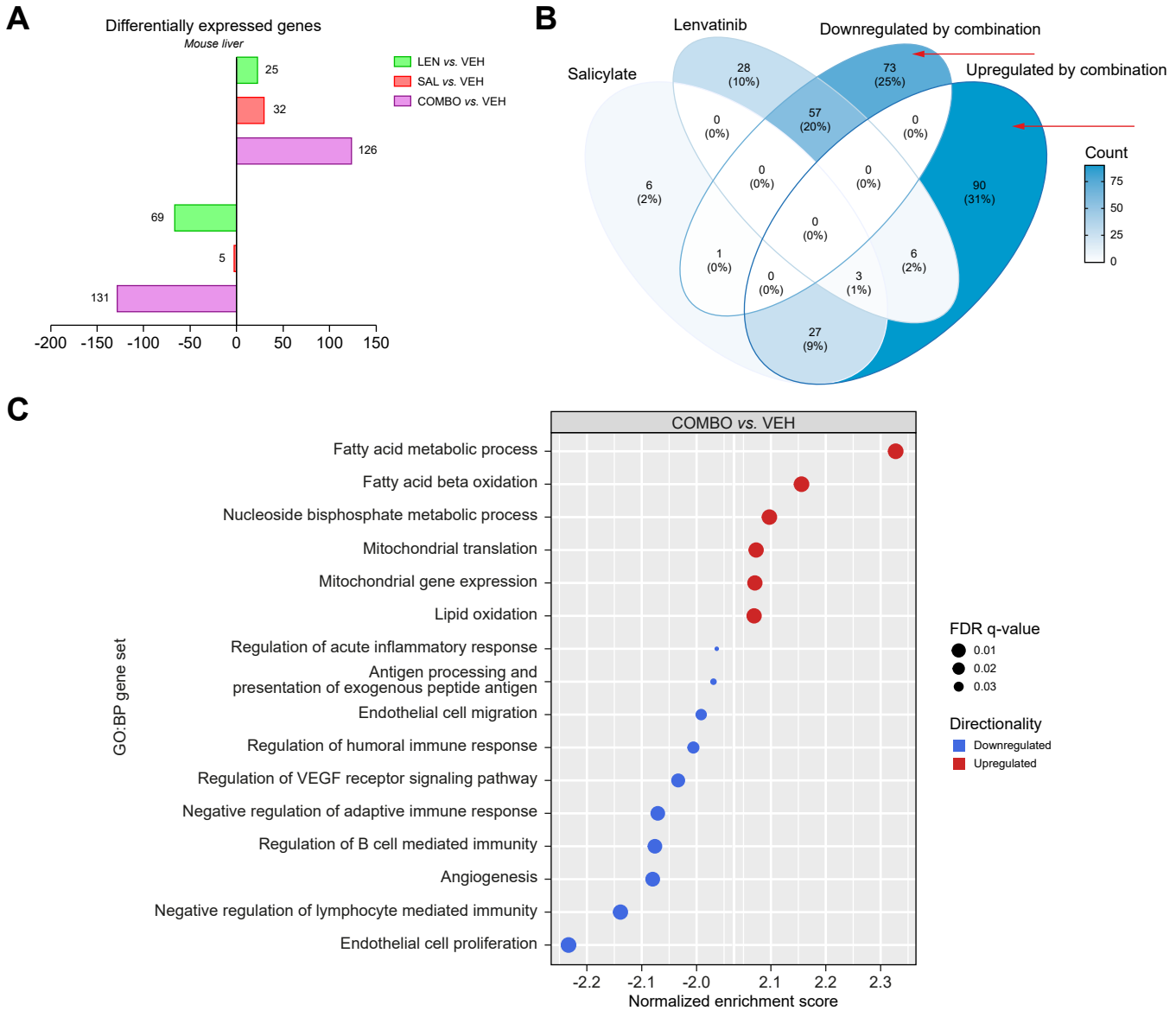

Fig. 6. COMBO increases fatty acid oxidation and suppresses angiogenesis pathways in livers from the FAT-MASH mouse model. Bulk RNA-sequencing was performed on livers of FAT-MASH mice. (A) Number of up- or downregulated DEGs for each treatment comparison. (B) Number of DEGs altered by each monotherapy or COMBO treatment; red arrows indicate genes uniquely altered by COMBO. (C) Gene terms significantly regulated by COMBO compared with VEH. All DEGs (A,B) and select significantly up- and downregulated gene terms (C) have an FDR q-value ≤0.05. All RNA-sequencing data are based on n = 6 technical replicates per treatment group. COMBO, lenvatinib + salsalate; DEG, differentially expressed gene; FDR, false discovery rate; MASH VEH, vehicle.

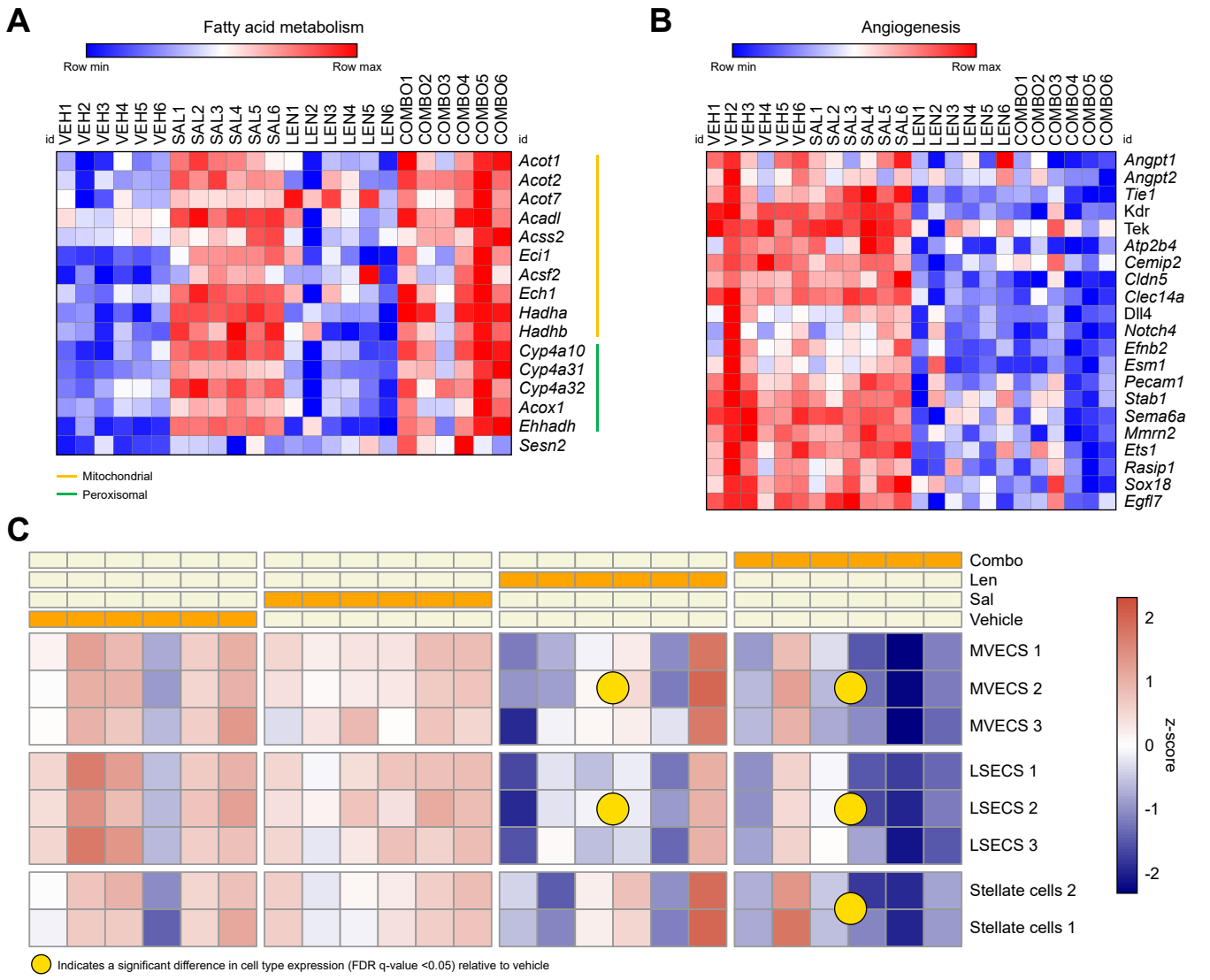

Fig. 7. Modulation of gene expression by COMBO therapy. Heatmaps demonstrating significantly differentially expressed genes in response to COMBO treatment (FDR q-value ≤0.05) for (A) fatty acid metabolism and (B) angiogenesis. (C) ssGSEA depicting significantly altered liver cell type signatures. All RNA-sequencing data are based on n = 6 technical replicates per treatment group. COMBO, lenvatinib + salsalate; FDR, false discovery rate; ssGSEA, single-sample gene set enrichment analysis.

Angpt2), and the angiopoietin receptors tyrosine kinase with immunoglobulin-like and EGF-like domains 1 (*Tie1*) and TEK receptor tyrosine kinase (*Tek/Tie2*) (Fig. 7B).

Cell type analysis using gene sets reported elsewhere[47] predicted that angiogenic and fibrotic cell types, such as liver sinusoidal endothelial cells (LSECs), which form the sinusoidal wall, and hepatic stellate cells (HSCs), which are responsible for collagen production, would be downregulated in response to COMBO (Fig. 7C; Figs. S5A and B). Specifically, downregulation of immune gene sets were linked to the suppression of Fcgrb2 (an inhibitor of B and other myeloid cells[48]), Clec4g (an activator of inflammatory responses and immune tolerance[49]), Cd55 and Cr2 (activators of the complement system[50,51]), and Fcer2a (a marker of B2 lymphocytes associated with the onset of steatohepatitis[52]) (Fig. S5C).

To identify putative transcriptional regulators that might be important for the beneficial effects of COMBO therapy, an exploratory *in silico* transcription factor enrichment analysis was conducted (iRegulon, KU Leuven[53]) in both the Hep3B and the MASH–liver RNA-seq datasets. Surprisingly, despite some differences in DEGs, the transcriptional regulators with the highest enrichment score for both datasets were the same, with COMBO predicted to increase many DEGs through activating transcription factor 3 (ATF3) and inhibit many DEGs through ETS-1 pro-oncogene-1 (ETS-1) (Fig. 8). Specifically, ATF3 was the predicted mediator for upregulated genes involved in FAO, cell cycle inhibition, and apoptosis (Fig. 8A,B), while suppression of growth, fibrosis, and endothelial cell proliferation were associated with the suppression of ETS1 (Fig. 8C,D). Importantly, consistent with the *in silico* analysis, ATF3 and ETS1 mRNA (Fig. 8E) and protein expression (Fig. 8F–H) were up- and downregulated, respectively in Hep3B cells under COMBO therapy. Taken together, these data indicate that oral delivery of a SAL + LEN combination in mice elicits favorable effects on

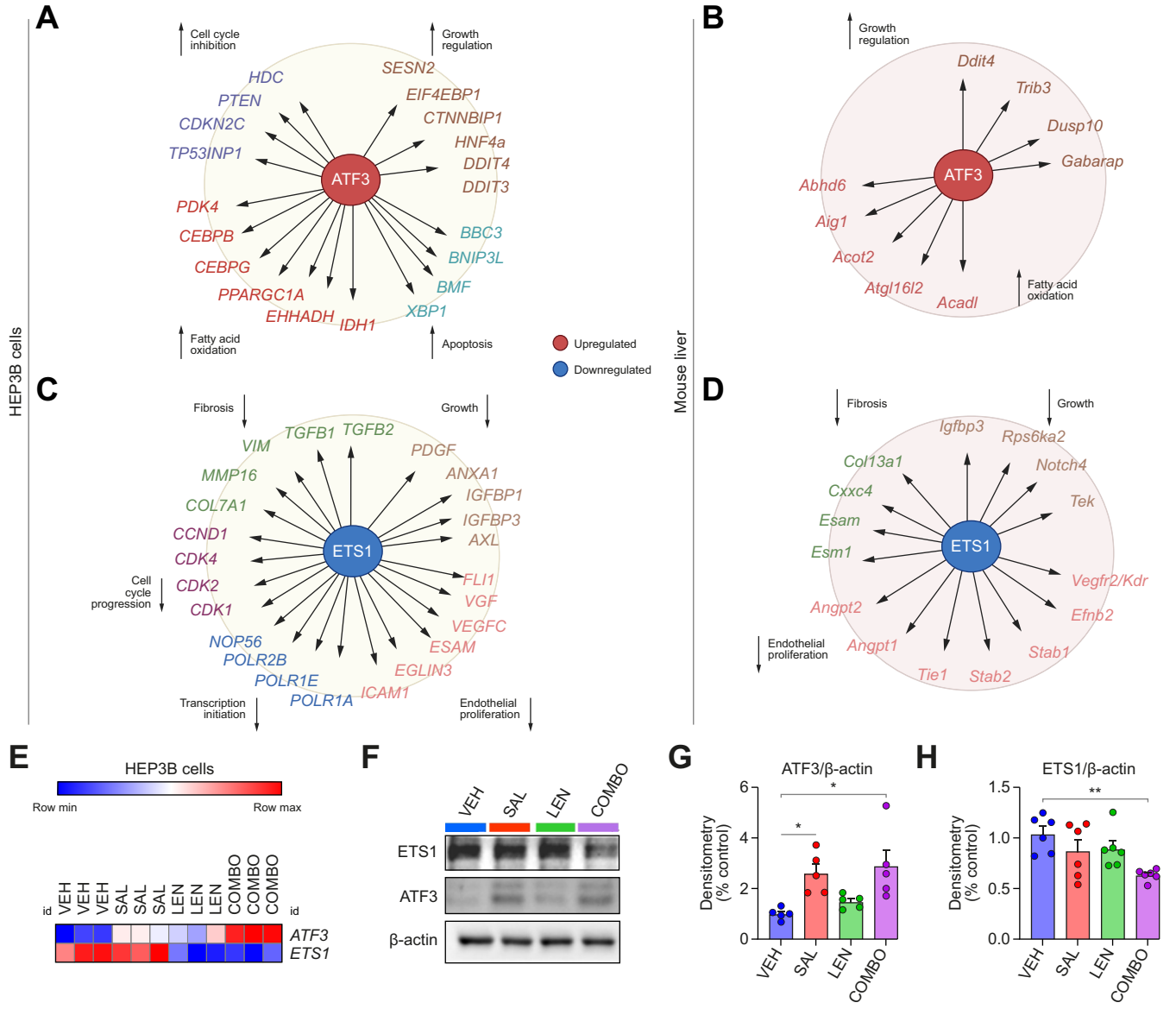

Fig. 8. COMBO therapy elicits changes in transcriptional activity potentially by increasing ATF3 and reducing ETS1. Key significantly upregulated transcription targets for (A,B) ATF3 and (C,D) ETS1 in COMBO-treated Hep3B cells or mouse liver tissue, respectively. (E) mRNA expression of *ATF3* and *ETS1* in treated Hep3B cells. (F) Representative immunoblotting in Hep3B cells following 24-h treatment with standard doses of each agent or COMBO and corresponding (G) ATF3 and (H) ETS1 total protein quantification. All RNA-sequencing data are based on n = 3 or n = 6 technical replicates per treatment group for Hep3B and liver data, respectively. Western blot data based on n = 3 experimental and n = 2 technical replicates; statistical significance determined via using one-way ANOVA with Tukey multiple comparisons (G–H); *$p \leq 0.05$, **$p \leq 0.01$. (A–D) created using BioRender (biorender.com). ATF3, activating transcription factor 3; COMBO, lenvatinib + salsalate; ETS1, ETS-proto-oncogene-1.

markers of liver steatosis, fibrosis, and angiogenesis, and broad transcriptional changes consistent with those observed in cultured Hep3B cells.

Discussion

To support protein synthesis required for elevated proliferation rates in HCC, the Warburg effect stimulates glycolysis and DNL, while FAO/β-oxidation is restricted.[54] We hypothesized that pairing clinically achievable doses of LEN with SAL (COMBO), would promote greater inhibition of tumor cell proliferation potentially through metabolic rewiring compared with either alone. Consistent with this hypothesis, we found that COMBO treatment inhibited the growth kinetics of cultured human HCC cell lines. When Hep3B cells were orthotopically implanted into the livers of mice, COMBO also extended median survival. Gene expression and post-transcriptional analysis demonstrated that COMBO suppressed transcriptional, translational, and cell cycle pathways to a greater extent than either agent alone. This was associated with SAL-driven inhibition of the mTOR-p70^{S6k} pathway, potentially mediated through AMPK-induced inhibitory phosphorylation of Raptor,[55] which was additive to the antiproliferative effects of LEN associated with the inhibition of tyrosine kinase receptors and

Erk activation.[56] HIF1α, a key transcriptional regulator of the Warburg effect associated with resistance to tyrosine kinase inhibitor therapy in advanced HCC,[54,57–60] was also inhibited by SAL and COMBO. Taken together, these data suggest that the unique molecular targets of SAL and LEN lead to synergistic inhibition of HCC proliferation, which could be involved in the improved survival of orthotopic HCC mice.

Further, resistance to therapy and reduced survival in MASH-driven HCC is characterized by a tumor promoting microenvironment resulting from the presence of liver steatosis and fibrosis. In the FAT-MASH model, COMBO therapy reduced NAS to a greater degree than either SAL or LEN alone. Our data suggest that LEN and SAL elicit dual-targeting on angiogenesis and fibrosis, respectively, which are important determinants of MASH severity and MASH-HCC prognosis.[9,61,62] Improvements in fibrosis, which is associated with poor immune surveillance in MASH-HCC,[9] were reduced by SAL and COMBO (Fig. 5). Consistent with distinct effects of both drugs, RNA-seq analysis revealed that COMBO was associated with reduced genetic signatures linked to LSECs and HSCs (Fig. 7C), cells that stimulate angiogenesis and fibrosis, respectively. Increased sheer stress in the steatotic liver prompts capillarization of LSECs and production of inflammatory signals,[63,64] which activates neighboring HSCs, resulting in fibrosis.[65–67] This work highlights that, at clinically relevant doses[21] (∼0.25% w/w), improvements in NAS can be attributed to LEN and SAL-mediated reductions in angiogenesis and fibrosis, respectively, highlighting the potential importance of this dual-targeting approach in managing MASH-HCC.

Lastly, we were keen to understand the transcriptional pathways that might be responsible for the pleiotropic benefits mediated by COMBO on tumor proliferation, metabolic rewiring, steatosis, angiogenesis, and fibrosis. COMBO increased the expression of ATF3 and reduced the expression of ETS1. Our analysis linking ATF3 with increased expression of transcripts controlling FAO and negative regulation of mTORC1 is consistent with previous studies.[68–71] Other studies reported increased MASH in ATF3-null mice, while its overexpression counteracts these effects.[72–74] By contrast, ETS1 is known to enhance the transcription of genes supporting angiogenesis, invasion, metastasis, and fibrosis[75,76] and epithelial–mesenchymal transition in cancer[75,76] in response to pro-angiogenic FGF and VEGF signals,[77,78] and was consistently reduced by COMBO in both cell and mouse datasets (Fig. 8). This coincided with COMBO-mediated reductions in fibrosis, analogous to those observed with ETS1 knockdown in the MCD mouse model of fibrosis.[79] Furthermore, our reductions in p-ERK and HIF1α, previously shown to increase ETS1 expression,[75,80] aligned with our observations of reduced ETS1 mRNA and protein in response to COMBO. Therefore, our data, in addition to existing literature, support the possibility that COMBO-mediated increases in ATF3 and reductions in ETS1 are important for reducing cell proliferation, steatosis, angiogenesis, and fibrosis. However, further loss-of-function studies are needed to confirm these findings as it is likely that multiple overlapping pathways exist. For example, COMBO also led to the acute activation of AMPK and subsequent phosphorylation of ACC. The phosphorylation and inhibition of ACC by AMPK has been shown to reduce MASH, fibrosis, and HCC development,[43,81] suggesting that this is also important for the potential beneficial effects of this approach.

Our study had several limitations. The lack of carcinogenesis and tumor growth in the FAT-MASH model limited our understanding of how SAL and LEN reduce tumor burden in the setting of MASH-HCC. In addition, the lack of temporal resolution in our xenograft model precluded our understanding of how COMBO-mediated mechanisms inhibit tumor kinetics. Future studies in which the tumor burden is monitored in FAT-MASH mice, potentially using magnetic resonance imaging or liver biopsy, would be beneficial to address both of these limitations.

In conclusion, this study demonstrates that the addition of SAL to LEN improved survival in a mouse model of HCC compared with LEN monotherapy and also reduced markers of liver steatosis, fibrosis, and angiogenesis in a mouse model of MASH. Although multiple mechanisms are important, COMBO elicited pronounced transcriptional reprogramming of liver tumor cells and normal liver parenchyma. Given that the interruption, reduction, and/or withdrawal of LEN because of adverse events are common in many patients with unresectable HCC,[8] the use of SAL could provide a means to reduce doses of LEN while still maximizing its therapeutic efficacy. Given the well tolerated and approved status of these therapeutics, our study provides a rationale for the further clinical development of LEN and SAL for patients with MASH-HCC.

Affiliations

[1]*Centre for Metabolism, Obesity and Diabetes Research, McMaster University, 1280 Main Street West, Hamilton, ONT, L8S 4K1, Canada;* [2]*Division of Endocrinology and Metabolism, Department of Medicine, McMaster University, 1280 Main Street West, Hamilton, ONT, L8S 4K1, Canada;* [3]*Juravinski Cancer Center, Hamilton Health Sciences, 699 Concession Street, Hamilton, ONT, L8V 5CV, Canada;* [4]*Department of Oncology, McMaster University, 1280 Main Street West, Hamilton, ONT, L8S 4K1, Canada*

Abbreviations

ACAD, acyl-CoA dehydrogenase; ACC, acetyl-CoA carboxylase; ACLY, ATP citrate lyase; ACSL, acetyl-CoA synthetase; AFP, alpha fetoprotein; AMPK, AMP-activated protein kinase; Angpt, angiopoietin; ASM, acid-soluble material; ATF3, activating transcription factor 3; ATF3, activating transcription factor 3; COMBO, combination of LEN + SAL; DEG, differentially expressed gene; Dll4, delta-like canonical notch ligand 4; DNL, de novo lipogenesis; DPMs, disintegrations per minute; E, embryonic day; EHHADH, enoyl-CoA hydratase and 3-hydroxyacyl-CoA dehydrogenase; ELO, elongase; ETS1, ETS-proto-oncogene-1; FAO, fatty acid oxidation; FDR, false discovery rate; GOBP, Gene Ontology Biological Process; GSEA, gene set enrichment analysis; GTF, general transcription factor; HADH, hydroxyacyl-CoA dehydrogenase; HCC, hepatocellular carcinoma; HIF1α, hypoxia inducible factor α; HK2, hexokinase; HSA, highest single agent; HSC, hepatic stellate cells; ITGA2, integrin subunit alpha 2; KO, knockout; LDHA, lactate dehydrogenase; LEN, lenvatinib; LSEC, liver sinusoidal endothelial cell; MASH, Metabolic dysfunction-associated steatohepatitis; MED, mediator complex subunit; MEFs, murine embryonic fibroblasts; NAS, nonalcoholic fatty liver disease activity score; NES, normalized enrichment score; p-S6, S6 phosphorylation at Ser240-244; p70S6k, p70 S6-kinase; PGK1, phosphoglycerate kinase; PKM, pyruvate kinase; POL, polymerase; PSR, Picrosirius Red; RNA-seq, RNA-sequencing; ROI, region of interest; RUNX1, RUNX family transcription factor 1; SAL, salsalate; ssGSEA, single-sample gene set enrichment analysis; TAF, TATA-box binding protein-associated factor; Tek/Tie2, TEK receptor tyrosine kinase; TGFB1, transforming growth factor beta 1; Tie1, tyrosine kinase with

immunoglobulin-like and EGF-like domains 1; Vegfr2/Kdr, vascular endothelial growth factor receptor 2; VEH, vehicle; VIM, vimentin; WME, William's E Medium; WT, wild-type.

Financial support

This work was supported by funding from the McMaster University Faculty of Health Sciences, Hamilton Health Sciences (HHS), and the Canadian Institutes of Health Research (CIHR).

Conflicts of interest

The authors declare no conflicts of interest that pertain to this work.

Please refer to the accompanying ICMJE disclosure forms for further details.

Authors' contributions

EET: methodology, investigation, writing – original draft, writing – review & editing. EA, JG, YRHS, JSVL, SW, FDP, CMV, DDR, O-DB: investigation. RF: data curation. BM, PM, TT, GRS: funding acquisition. GRS: supervision, writing – review & editing.

Data availability statement

The data that support the findings of this study are available upon request from the corresponding author and via GEO accession no. GSE282660.

Supplementary data

Supplementary data to this article can be found online at https://doi.org/10.1016/j.jhepr.2025.101354.

References

Author names in bold designate shared co-first authorship

[1] Baffy G, Brunt EM, Caldwell SH. Hepatocellular carcinoma in non-alcoholic fatty liver disease: an emerging menace. J Hepatol 2012;56:1384–1391.
[2] Duan XY, Zhang L, Fan JG, et al. NAFLD leads to liver cancer: do we have sufficient evidence? Cancer Lett 2014;345:230–234.
[3] Akinyemiju T, Abera S, Ahmed M, et al. The burden of primary liver cancer and underlying etiologies from 1990 to 2015 at the global, regional, and national level: results from the Global Burden of Disease Study 2015. JAMA Oncol 2017;3:1683–1691.
[4] Estes C, Anstee QM, Arias-Loste MT, et al. Modeling NAFLD disease burden in China, France, Germany, Italy, Japan, Spain, United Kingdom, and United States for the period 2016-2030. J Hepatol 2018;69:896–904.
[5] Llovet JM, Kelley RK, Villanueva A, et al. Hepatocellular carcinoma. Nat Rev Dis Primers 2021;7(6).
[6] **Pinyol R**, **Torrecilla S**, Wang H, et al. Molecular characterisation of hepatocellular carcinoma in patients with non-alcoholic steatohepatitis. J Hepatol 2021;75:865–878.
[7] Finn RS, Qin S, Ikeda M, et al. Atezolizumab plus bevacizumab in unresectable hepatocellular carcinoma. N Engl J Med 2020;382:1894–1905.
[8] Kudo M, Finn RS, Qin S, et al. Lenvatinib versus sorafenib in first-line treatment of patients with unresectable hepatocellular carcinoma: a randomised phase 3 non-inferiority trial. Lancet 2018;391:1163–1173.
[9] Pfister D, Nunez NG, Pinyol R, et al. NASH limits anti-tumour surveillance in immunotherapy-treated HCC. Nature 2021;592:450–456.
[10] **Kelley RK**, **Rimassa L**, Cheng AL, et al. Cabozantinib plus atezolizumab versus sorafenib for advanced hepatocellular carcinoma (COSMIC-312): a multicentre, open-label, randomised, phase 3 trial. Lancet Oncol 2022;23:995–1008.
[11] **Rimini M**, **Rimassa L**, Ueshima K, et al. Atezolizumab plus bevacizumab versus lenvatinib or sorafenib in non-viral unresectable hepatocellular carcinoma: an international propensity score matching analysis. ESMO Open 2022;7:100591.
[12] **Casadei-Gardini A**, **Rimini M**, Tada T, et al. Atezolizumab plus bevacizumab versus lenvatinib for unresectable hepatocellular carcinoma: a large real-life worldwide population. Eur J Cancer 2023;180:9–20.
[13] Preston SJ, Arnold MH, Beller EM, et al. Comparative analgesic and anti-inflammatory properties of sodium salicylate and acetylsalicylic acid (aspirin) in rheumatoid arthritis. Br J Clin Pharmacol 1989;27:607–611.
[14] Steinberg GR, Dandapani M, Hardie DG. AMPK: mediating the metabolic effects of salicylate-based drugs? Trends Endocrinol Metab 2013;24:481–487.
[15] Fleischman A, Shoelson SE, Bernier R, et al. Salsalate improves glycemia and inflammatory parameters in obese young adults. Diabetes Care 2008;31:289–294.
[16] Faghihimani E, Amini M, Adibi A, et al. Evaluating the efficacy of Salsalate on prediabetic and diabetic patients with fatty liver: a randomized clinical trial. J Res Pharm Pract 2013;2:40–43.
[17] Goldfine AB, Conlin PR, Halperin F, et al. A randomised trial of salsalate for insulin resistance and cardiovascular risk factors in persons with abnormal glucose tolerance. Diabetologia 2013;56:714–723.
[18] Goldfine AB, Fonseca V, Jablonski KA, et al. Salicylate (salsalate) in patients with type 2 diabetes: a randomized trial. Ann Intern Med 2013;159:1–12.
[19] Hauser TH, Salastekar N, Schaefer EJ, et al. Effect of targeting inflammation with salsalate: the TINSAL-CVD randomized clinical trial on progression of coronary plaque in overweight and obese patients using statins. JAMA Cardiol 2016;1:413–423.
[20] Goldfine AB, Fonseca V, Jablonski KA, et al. The effects of salsalate on glycemic control in patients with type 2 diabetes: a randomized trial. Ann Intern Med 2010;152:346–357.
[21] Smith BK, Ford RJ, Desjardins EM, et al. Salsalate (salicylate) uncouples mitochondria, improves glucose homeostasis, and reduces liver lipids independent of AMPK-beta1. Diabetes 2016;65:3352–3361.
[22] Hawley SA, Fullerton MD, Ross FA, et al. The ancient drug salicylate directly activates AMP-activated protein kinase. Science 2012;336:918–922.
[23] Garcia D, Hellberg K, Chaix A, et al. Genetic liver-specific AMPK activation protects against diet-induced obesity and NAFLD. Cell Rep 2019;26:192–208.
[24] Cusi K, Alkhouri N, Harrison SA, et al. Efficacy and safety of PXL770, a direct AMP kinase activator, for the treatment of non-alcoholic fatty liver disease (STAMP-NAFLD): a randomised, double-blind, placebo-controlled, phase 2a study. Lancet Gastroenterol Hepatol 2021;6:889–902.
[25] Steinberg GR, Hardie DG. New insights into activation and function of the AMPK. Nat Rev Mol Cell Biol 2023;24:255–272.
[26] O'Brien AJ, Villani LA, Broadfield LA, et al. Salicylate activates AMPK and synergizes with metformin to reduce the survival of prostate and lung cancer cells ex vivo through inhibition of de novo lipogenesis. Biochem J 2015;469:177–187.
[27] **Broadfield LA**, **Marcinko K**, Tsakiridis E, et al. Salicylate enhances the response of prostate cancer to radiotherapy. Prostate 2019;79:489–497.
[28] **Tsakiridis EE**, **Broadfield L**, **Marcinko K**, et al. Combined metformin-salicylate treatment provides improved anti-tumor activity and enhanced radiotherapy response in prostate cancer; drug synergy at clinically relevant doses. Transl Oncol 2021;14:101209.
[29] Houde VP, Donzelli S, Sacconi A, et al. AMPK beta1 reduces tumor progression and improves survival in p53 null mice. Mol Oncol 2017;11:1143–1155.
[30] Morrow MR, Batchuluun B, Wu J, et al. Inhibition of ATP-citrate lyase improves NASH, liver fibrosis, and dyslipidemia. Cell Metab 2022;34:919–936.
[31] Endo M, Honda K, Saito T, et al. Maximum plasma concentration of lenvatinib is useful for predicting thrombocytopenia in patients treated for hepatocellular carcinoma. World J Oncol 2021;12:165–172.
[32] **Tsuchida T**, **Lee YA**, Fujiwara N, et al. A simple diet- and chemical-induced murine NASH model with rapid progression of steatohepatitis, fibrosis and liver cancer. J Hepatol 2018;69:385–395.
[33] Takahashi Y, Fukusato T. Histopathology of nonalcoholic fatty liver disease/nonalcoholic steatohepatitis. World J Gastroenterol 2014;20:15539–15548.
[34] Lambertucci F, Li S, Motino O, et al. Orthotopic model of hepatocellular carcinoma in mice. Methods Mol Biol 2024;2769:1–13.
[35] Johnson P, Zhou Q, Dao DY, et al. Circulating biomarkers in the diagnosis and management of hepatocellular carcinoma. Nat Rev Gastroenterol Hepatol 2022;19:670–681.
[36] Ali A, Mekhaeil B, Biziotis OD, et al. The SGLT2 inhibitor canagliflozin suppresses growth and enhances prostate cancer response to radiotherapy. Commun Biol 2023;6:919.
[37] Liston DR, Davis M. Clinically relevant concentrations of anticancer drugs: a guide for nonclinical studies. Clin Cancer Res 2017;23:3489–3498.
[38] Crosio C, Fimia GM, Loury R, et al. Mitotic phosphorylation of histone H3: spatio-temporal regulation by mammalian Aurora kinases. Mol Cell Biol 2002;22:874–885.
[39] **Ahn JII**, **Zhang L**, Ravishankar H, et al. Architectural basis for cylindrical self-assembly governing Plk4-mediated centriole duplication in human cells. Commun Biol 2023;6:712.
[40] **Sumara I**, **Vorlaufer E**, Stukenberg PT, et al. The dissociation of cohesin from chromosomes in prophase is regulated by Polo-like kinase. Mol Cell 2002;9:515–525.

[41] **Faubert B**, **Vincent EE**, Poffenberger MC, et al. The AMP-activated protein kinase (AMPK) and cancer: many faces of a metabolic regulator. Cancer Lett 2015;356:165–170.
[42] **Dzamko N**, **van Denderen BJ**, Hevener AL, et al. AMPK beta1 deletion reduces appetite, preventing obesity and hepatic insulin resistance. J Biol Chem 2010;285:115–122.
[43] **Lally JSV**, **Ghoshal S**, DePeralta DK, et al. Inhibition of acetyl-CoA carboxylase by phosphorylation or the inhibitor ND-654 suppresses lipogenesis and hepatocellular carcinoma. Cell Metab 2019;29:174–182.
[44] Esquejo RM, Salatto CT, Delmore J, et al. Activation of liver AMPK with PF-06409577 corrects NAFLD and lowers cholesterol in rodent and primate preclinical models. EBioMedicine 2018;31:122–132.
[45] Llovet JM, Willoughby CE, Singal AG, et al. Nonalcoholic steatohepatitis-related hepatocellular carcinoma: pathogenesis and treatment. Nat Rev Gastroenterol Hepatol 2023;20:487–503.
[46] **Vacca M**, **Kamzolas I**, **Harder LM**, et al. An unbiased ranking of murine dietary models based on their proximity to human metabolic dysfunction-associated steatotic liver disease (MASLD). Nat Metab 2024;6:1178–1196.
[47] Aizarani N, Saviano A, Sagar, et al. A human liver cell atlas reveals heterogeneity and epithelial progenitors. Nature 2019;572:199–204.
[48] Smith KG, Clatworthy MR. FcgammaRIIB in autoimmunity and infection: evolutionary and therapeutic implications. Nat Rev Immunol 2010;10:328–343.
[49] **Backdahl L**, **Aoun M**, Norin U, et al. Identification of Clec4b as a novel regulator of bystander activation of auto-reactive T cells and autoimmune disease. Plos Genet 2020;16:e1008788.
[50] **Ozen A**, **Comrie WA**, **Ardy RC**, et al. CD55 deficiency, early-onset protein-losing enteropathy, and thrombosis. N Engl J Med 2017;377:52–61.
[51] Ward T, Pipkin PA, Clarkson NA, et al. Decay-accelerating factor CD55 is identified as the receptor for echovirus 7 using CELICS, a rapid immunofocal cloning method. EMBO J 1994;13:5070–5074.
[52] Bruzzi S, Sutti S, Giudici G, et al. B2-Lymphocyte responses to oxidative stress-derived antigens contribute to the evolution of nonalcoholic fatty liver disease (NAFLD). Free Radic Biol Med 2018;124:249–259.
[53] **Janky R**, **Verfaillie A**, Imrichova H, et al. iRegulon: from a gene list to a gene regulatory network using large motif and track collections. Plos Comput Biol 2014;10:e1003731.
[54] Yang F, Hilakivi-Clarke L, Shaha A, et al. Metabolic reprogramming and its clinical implication for liver cancer. Hepatology 2023;78:1602–1624.
[55] Steinberg GR, Carling D. AMP-activated protein kinase: the current landscape for drug development. Nat Rev Drug Discov 2019;18:527–551.
[56] Vogel A, Qin S, Kudo M, et al. Lenvatinib versus sorafenib for first-line treatment of unresectable hepatocellular carcinoma: patient-reported outcomes from a randomised, open-label, non-inferiority, phase 3 trial. Lancet Gastroenterol Hepatol 2021;6:649–658.
[57] Sakamoto T, Weng JS, Hara T, et al. Hypoxia-inducible factor 1 regulation through cross talk between mTOR and MT1-MMP. Mol Cell Biol 2014;34:30e42.
[58] Shen YC, Ou DL, Hsu C, et al. Activating oxidative phosphorylation by a pyruvate dehydrogenase kinase inhibitor overcomes sorafenib resistance of hepatocellular carcinoma. Br J Cancer 2013;108:72–81.
[59] Tesori V, Piscaglia AC, Samengo D, et al. The multikinase inhibitor Sorafenib enhances glycolysis and synergizes with glycolysis blockade for cancer cell killing. Sci Rep 2015;5:9149.
[60] Reyes R, Wani NA, Ghoshal K, et al. Sorafenib and 2-deoxyglucose synergistically inhibit proliferation of both sorafenib-sensitive and -resistant HCC cells by inhibiting ATP production. Gene Expr 2017;17:129–140.
[61] Lei L, Ei Mourabit H, Housset C, et al. Role of angiogenesis in the pathogenesis of NAFLD. J Clin Med 2021;10:1338.
[62] **Yao C**, **Wu S**, Kong J, et al. Angiogenesis in hepatocellular carcinoma: mechanisms and anti-angiogenic therapies. Cancer Biol Med 2023;20:25–43.
[63] Hammoutene A, Rautou PE. Role of liver sinusoidal endothelial cells in non-alcoholic fatty liver disease. J Hepatol 2019;70:1278–1291.
[64] **Verhulst S**, **van Os EA**, De Smet V, et al. Gene signatures detect damaged liver sinusoidal endothelial cells in chronic liver diseases. Front Med 2021;8:750044.
[65] Deleve LD, Wang X, Guo Y. Sinusoidal endothelial cells prevent rat stellate cell activation and promote reversion to quiescence. Hepatology 2008;48:920–930.
[66] Xie G, Wang X, Wang L, et al. Role of differentiation of liver sinusoidal endothelial cells in progression and regression of hepatic fibrosis in rats. Gastroenterology 2012;142:918–927.
[67] Tsuchida T, Friedman SL. Mechanisms of hepatic stellate cell activation. Nat Rev Gastroenterol Hepatol 2017;14:397–411.
[68] Wang Y, Nakajima T, Gonzalez FJ, et al. PPARs as metabolic regulators in the liver: lessons from liver-specific PPAR-null mice. Int J Mol Sci 2020;21:2061.
[69] **Zhang L**, **Zhang Y**, **Chang X**, et al. Imbalance in mitochondrial dynamics induced by low PGC-1alpha expression contributes to hepatocyte EMT and liver fibrosis. Cell Death Dis 2020;11:226.
[70] DeYoung MP, Horak P, Sofer A, et al. Hypoxia regulates TSC1/2-mTOR signaling and tumor suppression through REDD1-mediated 14-3-3 shuttling. Genes Dev 2008;22:239–251.
[71] Lu C, Jiang Y, Xu W, et al. Sestrin2: multifaceted functions, molecular basis, and its implications in liver diseases. Cell Death Dis 2023;14:160.
[72] **Cheng CF**, **Ku HC**, **Cheng JJ**, et al. Adipocyte browning and resistance to obesity in mice is induced by expression of ATF3. Commun Biol 2019;2:389.
[73] Xu Y, Hu S, Jadhav K, et al. Hepatocytic activating transcription factor 3 protects against steatohepatitis via hepatocyte nuclear factor 4alpha. Diabetes 2021;70:2506–2517.
[74] Xiaoyan L, Shengbing Z, Yu Z, et al. Low expression of activating transcription factor 3 in human hepatocellular carcinoma and its clinicopathological significance. Pathol Res Pract 2014;210:477–481.
[75] Dittmer J. The role of the transcription factor Ets1 in carcinoma. Semin Cancer Biol 2015;35:20–38.
[76] Rodgers JJ, McClure R, Epis MR, et al. ETS1 induces transforming growth factor beta signaling and promotes epithelial-to-mesenchymal transition in prostate cancer cells. J Cell Biochem 2019;120:848–860.
[77] Iwasaka C, Tanaka K, Abe M, et al. Ets-1 regulates angiogenesis by inducing the expression of urokinase-type plasminogen activator and matrix metalloproteinase-1 and the migration of vascular endothelial cells. J Cell Physiol 1996;169:522–531.
[78] **Chen J**, **Fu Y**, **Day DS**, et al. VEGF amplifies transcription through ETS1 acetylation to enable angiogenesis. Nat Commun 2017;8:383.
[79] **Liu D**, **Wang K**, Li K, et al. Ets-1 deficiency alleviates nonalcoholic steatohepatitis via weakening TGF-beta1 signaling-mediated hepatocyte apoptosis. Cell Death Dis 2019;10:458.
[80] Zhang LY, Tan Y, Luo XJ, et al. The roles of ETS transcription factors in liver fibrosis. Hum Cell 2023;36:528–539.
[81] Batchuluun B, Pinkosky SL, Steinberg GR. Lipogenesis inhibitors: therapeutic opportunities and challenges. Nat Rev Drug Discov 2022;21:283–305.

Keywords: Lipogenesis; Salicylic acid; Metabolic dysfunction-associated steatohepatitis.
Received 9 August 2024; received in revised form 23 January 2025; accepted 6 February 2025; Available online 14 February 2025